Received: 1 October 2021 | Revised: 26 February 2022 | Accepted: 3 March 2022

DOI: 10.1002/bmc.5362

RESEARCH ARTICLE

Biomedical Chromatography WILEY

Metabonomics study on the hepatoprotective effect mechanism of polysaccharides from different processed products of *Angelica sinensis* on layer chickens based on UPLC–Q/TOF–MS/MS, multivariate statistical analysis and conjoint analysis

Fan-lin Wu | **Yong-hao Hu** | **Peng Ji** | **Chen-chen Li** | **Jian He**

College of Veterinary Medicine, Gansu Agricultural University, Lanzhou, China

Correspondence
Yong-hao Hu and Peng Ji, No. 1, Yingmen village, Anning district, Lanzhou city, Gansu Province, China.
Email: yhh0817@126.com and jipengjipeng528@163.com

Funding information
University-level Fuxi talent project, Grant/Award Number: Gaufx-02Y05; National Natural Science Foundation of China, Grant/Award Number: 31602102; Lanzhou talent innovation and entrepreneurship project, Grant/Award Number: 2021-RC-57

Abstract

Chicken colibacillosis is one of the most severe diseases in the poultry industry. Ceftiofur sodium (CS) is often used to treat it in clinical practice and lipopolysaccharide (LPS) accumulates in the chicken's body. Previous experimental studies found that CS combined with LPS could induce liver injury in layer chickens, and polysaccharides from charred *Angelica sinensis*(CASP) had a better hepatoprotective effect than polysaccharides from unprocessed *Angelica sinensis*(UASP). However, the intervention mechanism was unclear. Thus, UPLC–Q/TOF–MS/MS-based metabonomics and transcriptomics were used in this study to clarify the hepatoprotective effect mechanism of CASP and UASP in layer chickens. Transcriptomics and enzyme-linked immunosorbent assay were used for biological verification of some critical mutual metabolic pathways screened with metabonomics. The comprehensive analysis results showed that in a layer chicken liver injury model built with LPS and CS, 12 critical metabolic pathways were disturbed, involving 10 important differential metabolites. The hepatoprotective effect mechanism of CASP is related to the arachidonic acid metabolism and mTOR signaling pathways, involving nine important differential metabolites. In contrast, the hepatoprotective effect mechanism of UASP is related to the arachidonic acid metabolism pathway, involving six important differential metabolites.

KEYWORDS
layer chickens, liver injury, LPS, metabonomics, polysaccharides from charred *Angelica sinensis* (CASP), polysaccharides from unprocessed *Angelica sinensis*(UASP)

Abbreviations: ALT, alanine aminotransferase; AS, *Angelica sinensis*; AST, aspartate aminotransferase; CASP, polysaccharides from charred *Angelica sinensis*; CC, chicken colibacillosis; CS, ceftiofur sodium; FC, fold change; LPS, lipopolysaccharide; PLS-DA, partial least squares-discriminant analysis; UASP, polysaccharides from unprocessed AS; UPLC–Q/TOF–MS/MS, ultra-performance liquid chromatography/quadrupole time-of-flight mass spectrometry/mass spectrometry; VIP, variable importance in projection; VN, Venn.

1 | INTRODUCTION

Chicken colibacillosis (CC) is an infectious disease caused by pathogenic *Escherichia coli* (Naghizadeh et al., 2019). To prevent and treat this disease, ceftiofur sodium (CS) is often used as the "Kai Kou" drug in the layer chicken industry. When CC is treated with CS, a considerable amount of lipopolysaccharide (LPS) is produced (Chang et al., 2020; Subramanian et al., 2008). Many studies have shown that LPS can induce liver injury, and some previous studies have found that CS combined with LPS can induce liver injury in layer chickens (Liu et al., 2020). However, the specific mechanism remains unclear.

Radix Angelica Sinensis (AS) is derived from the dried roots of *Angelica sinensis* (Oliv.), a famous medicinal plant in Minxian County, Gansu Province, China (Wang et al., 2020). The temperament of AS is warm, and the taste is sweet and spicy. One of the meridian tropisms of AS is the liver. The effects of AS include replenishing blood (Yang et al., 2021), promoting blood circulation (Yuan et al., 2019) and anti-inflammation (Hua et al., 2019). Polysaccharide is an essential active component in AS. The polysaccharides from AS have significant immunological enhancement and antioxidant effects (Yu et al., 2013). Previous studies have found that the components of AS significantly changed after charring (Tao et al., 2017) and the hepatoprotective effect of polysaccharides from charred AS (CASP) was better than that of polysaccharides from unprocessed AS (UASP). However, the hepatoprotective effect mechanisms of CASP remain unclear.

Metabonomics, an important omics research technology, can mainly explain the pathological and drug intervention mechanisms by analyzing the differences in the types and contents of metabolites. Targeted and non-targeted metabonomics are two kinds of analytical techniques. Between them, the coverage of detected metabolites of non-targeted metabolomics is extensive. The detection technologies of metabonomics mainly include gas chromatography–mass spectrometry (GC–MS), ultra-performance liquid chromatography/quadrupole time-of-flight mass spectrometry/mass spectrometry (UPLC–Q/TOF–MS/MS) and nuclear magnetic resonance. Among these detection technologies, UPLC–Q/TOF–MS/MS has the advantages of high sensitivity and high resolution (Wan et al., 2020; Zhang, Chen et al., 2020; Zhang, Shi et al., 2020).

UPLC–Q/TOF–MS/MS-based metabonomics, transcriptomics technology and enzyme-linked immunosorbent assay (ELISA) were used in this study to explore the liver injury mechanism in layer chickens caused by CS combined with LPS and analyze the differences in the intervention mechanisms of UASP and CASP. This study can lay a foundation for research and development on new hepatoprotective drugs for layer chickens and has importance for reducing and substituting the use of antibiotics for a green and healthy livestock and poultry breeding industry.

2 | MATERIALS AND METHODS

2.1 | Reagents and instruments

An AB triple TOF 5600/6600 mass spectrometer (AB SCIEX), an Agilent 1290 infinity LC ultra-high-pressure liquid chromatography (Agilent) and a low-temperature high-speed centrifuge (Eppendorf 5430R) were used. The chromatographic columns used were a Waters Acquity UPLC BEH Amide 1.7 μm, 2.1 × 100 mm and a Waters Acquity UPLC HSS T3 1.8 μm, 2.1 × 100 mm. The solvents were acetonitrile (Merck, no. 1499230-935) and acetic acid (Sigma, 70221).

2.2 | Experimental materials

Polysaccharides from CASP and polysaccharides from UASP were made in our laboratory. Ceftiofur sodium was supplied by Qilu Animal Health Products Co. Ltd. LPS (*E. coli* O78) was made in our laboratory. Ninety-four 1-day-old laying chickens were purchased from Beijing Huadu Yukou Poultry Industry Co. Ltd.

2.3 | Methods

2.3.1 | The preliminary animal experiment program and sampling

A total of 94 one-day-old laying chickens had ad libitum access to feed and drinking water for 3 days. Then, 14 laying chickens were randomly selected as the control group and 16 others were selected as the model group (including two time points of blood collection, 6 and 48 h). The rest of the laying chickens were randomly divided into four groups (low- and high-dose intervention groups of UASP and CASP—0.125 and 0.25 g/kg/day), with 16 laying chickens in each group. The above doses were based on the pre-experiment results (He, 2019). The intervention groups were given different doses of the corresponding polysaccharides once a day for 10 days. On days 8 and 10, laying chickens in the model and other intervention groups were subcutaneously injected with CS (5 mg/kg) in the neck. Those in the control group were subcutaneously injected with the same amount of normal saline at the same time. Except for the control group, the chickens were injected with self-made LPS (4 ml/kg) after CS injection on day 10 of the experiment. Those in the control group were injected with the same amount of normal saline at the same time. The chickens were observed daily for abnormal reactions during the experiment. After the experiment, blood was collected from the heart of chickens from all of the groups after anesthesia. Liver tissue of chickens from all of the groups was collected and frozen at −80°C for later use. The serum was then prepared and frozen at −80°C for later use.

The subsequent experimental analysis materials of this study were the serum and liver tissue samples frozen at −80°C. The experimental materials included serum samples from the high-dose intervention group of CASP (CASPG, six samples at 6 and 48 h after modeling), the high-dose intervention group of UASP (UASPG, six samples at 6 and 48 h after modeling), the model group (six samples at 6 and 48 h after modeling) and the control group (six samples).

2.3.2 | Metabonomics detection and analysis

Preparation of quality control samples

Quality control (QC) was carried out in the experiment. The experimental data were evaluated through QCs to ensure that the metabolic spectrum difference obtained in the experiment reflected the biological differences between the samples. Quality control is important in metabonomics detection and analysis. Generally, a QC sample is a mixed sample made up of equal amounts of all of the samples, which is tested on the machine before, during and after LC–MS/MS injection of the sample to be tested. Therefore the test serum samples were mixed equally to prepare the QC samples. The stability of the instrument status and data was monitored and judged by comparison of total ion current chromatograms (TICs) of QC samples, the clustering of QC samples in principal component analysis (PCA), Pearson correlation analysis of QC samples, Hotelling's T^2 test and a multivariable control chart.

Sample pretreatment method

The serum samples were taken out of the −80°C freezer and slowly dissolved at 4°C. Samples of 100 μl from the chickens in each group were then taken, and precooled methanol acetonitrile solution (400 μl) was added (v/v = 1:1). The tubes were vortexed for 1 min, incubated at −20°C for 60 min and then centrifuged for 20 min (4°C, 14,000 rcf) (Gao et al., 2021; Zhang et al., 2019). The supernatant was freeze-dried and stored at −80°C.

UPLC–Q/TOF–MS/MS analysis

1. Chromatographic conditions

The samples were separated by ultra-performance liquid chromatography (UPLC) with a hydrophilic interaction chromatography (HILIC) column (Agilent 1290). The column temperature was 25°C and the flow rate was 0.3 ml/min. The mobile phase comprised (A) water + 25 mM ammonium acetate + 25 mM ammonia water and (B) acetonitrile. The gradient elution procedure was as follows: 0–1 min, 95% B; 1–14 min, B changed linearly from 95 to 65%; 14–16 min, B changed linearly from 65 to 40%; 16–18 min, B stabilized at 40%; 18–18.1 min, B changed linearly from 40 to 95%; 18.1–23 min, B maintained at 95%. The samples were placed in a 4°C automatic sampler during the entire analysis process. The continuous analysis of samples was randomly conducted. Quality control samples were then inserted into the sample queue to monitor and evaluate the stability of the system and the reliability of the experimental data.

2. Q/TOF–MS/MS conditions

The samples were detected using the positive- and negative ions of electrospray ionization. The samples were separated by UPLC and analyzed using a triple TOF 5600 mass spectrometer (AB SCIEX). The electrospray ionization source conditions after HILIC chromatography were as follows: ion source gas 1, 60; ion source gas 2, 60; curtain gas, 30; source temperature, 600°C; ionspray voltage floating, ±5,500 V (positive and negative modes); TOF MS scan *m/z* range, 60–1,000 Da; product ion scan *m/z* range, 25–1,000 Da; TOF MS scan accumulation time, 0.20 s/spectra; product ion scan accumulation time, 0.05 s/spectra. The secondary mass spectrometry was obtained by information-dependent acquisition and a high-sensitivity model was adopted. Other conditions included the following: declustering potential, ±60 V (positive and negative modes) and collision energy, 35 ± 15 eV. The information-dependent acquisition was set as follows: excluding isotopes within 4 Da; candidate ions to monitor per cycle, 6.

Screening and identification of metabolites

The original data were converted into .mzXML format using ProteoWizard, and then the peak alignment, retention time correction and peak area extraction were performed using the XCMS program. After the pretreatment with Pareto scaling, multidimensional and one-dimensional statistical analyses were then used to screen the different metabolites, including unsupervised principal component analysis (PCA), supervised partial least squares discriminant analysis (PLS-DA) and orthogonal partial least squares discriminant analysis (OPLS-DA). One-dimensional statistical analysis methods (including Student's *t*-test and variation multiple analysis) were used to analyze the data, and the volcano map was drawn using R software.

The metabolites were identified by accurate mass number matching (<25 ppm) and secondary mass spectrum matching. They were identified by searching the database of standards established by the laboratory. Three standards assisted the detailed qualitative process of metabolites: (a) the experimental spectrum obtained by the high-resolution mass spectrometer was matched with the standard database and the quality accuracy was within 25 ppm; (b) the second-level mass spectrum was matched with high accuracy, which was not only based on the first-level mass spectrum, and the qualitative results were above those for level 2; and (c) the retention time reduced the false positives and improved the qualitative accuracy of biomarkers in the complex biological samples.

Correlation analysis of different metabolites

Correlation analysis can help measure the extent of correlation between metabolites with significant differences and further understand the relationship between metabolites in the process of biological state change.

Enrichment analysis of differential metabolic pathways

The Kyoto Encyclopedia of Genes and Genomes (KEGG) is a commonly used database in pathway research. The KEGG pathway enrichment analysis examines and calculates the significance level of metabolite enrichment of each pathway through Fisher's exact test to determine the significantly affected metabolic and signal transduction pathways. The enrichment of the KEGG pathway is generally significant when the *p*-value in the enrichment results is <0.05. The number of differentially expressed metabolites in the KEGG pathway reflects the influence of biological treatment on each pathway in the experimental design to some extent.

2.3.3 | Biological verification

Transcriptomics and ELISA were used to make a biological verification of some important mutual metabolic pathways screened with metabonomics.

Transcriptomics detection and analysis

Total RNA was extracted from the liver tissues (60 mg) using Trizol (Invitrogen, Carlsbad, CA, USA) according to the instruction manual. Subsequently, total RNA was qualified and quantified with Nano Drop and an Agilent 2100 bioanalyzer (Thermo Fisher Scientific, MA, USA). Then the mRNA library was constructed. The final library was amplified with phi29 to make a DNA nanoball, with more than 300 copies of one molecule. The DNA nanoballs were loaded into the patterned nanoarray, and 100 paired-end bases reads were generated on the BGIseq500 platform (BGI-Shenzhen, China).

The raw transcriptomic detection data were first filtered using the SOAPnuke software (v1.5.2) according to the following steps: removing reads containing sequencing adapters, removing reads whose low-quality base ratio (base quality ≤5.00) was >20% and removing reads with an unknown base ('N' base) ratio >5%. Then clean reads were obtained and stored in FASTQ format. The clean reads were mapped to the reference genome with HISAT2 (v2.0.4) software. Then Ericscript (v0.5.5) and rMATS (V3.2.5) were used for fusion genes and differential splicing genes, respectively. The software Bowtie2 (v2.2.5) was used to align the clean reads to the gene set, a database for this organism built using the software of BGI, with known and novel coding transcripts included, then the expression level of the gene was calculated using RSEM (v1.2.12) software. According to the gene expression in different experimental group samples, the heatmap was drawn using the heatmap software (v1.0.8). Essentially, differential expression analysis was performed using DESeq2(v1.4.5) software with a *Q*-value of ≤0.05. Gene Ontology (http://www.geneontology.org/) and KEGG (https://www.kegg.jp/) enrichment analyses of annotated different expression genes were performed using Phyper (https://en.wikipedia.org/wiki/Hypergeometric_distribution) based on the hypergeometric test to obtain insight into the changes in phenotype. The significance levels of terms and pathways were corrected using a *Q*-value of ≤0.05 with the Bonferroni software.

ELISA detection and analysis

The metabolite and protein contents in the chicken serum samples from the different experimental groups were validated with ELISA kits (Shanghai Enzyme-linked Biotechnology Co. Ltd) according to the kit instructions.

3 | RESULTS AND DISCUSSION

3.1 | Metabonomics detection and analysis results

3.1.1 | Quality control analysis

A series of QC analysis results (including the TIC graph, PCA, Hotelling's T^2 analysis, correlation analysis and multivariable control chart analysis) are shown in Figure S1. The figure reveals the stability and reliability of the instrumental analysis system. Moreover, the metabolic spectrum differences obtained in the experiment reflect the biological differences among the samples. These results reflect the necessity of QC analysis to some extent (Sánchez-Illana et al., 2018), and many metabonomics research works have confirmed that the QC analysis method can be used to control the quality of the original data to ensure that all data differences come from the sample itself rather than baseline drift during the experiment (Ding et al., 2022; Li et al., 2020; Wang et al., 2021; Xu et al., 2020; Zhang, Chen, et al., 2020)

3.1.2 | Typical metabolic graph and PCA score plot of each group

1. Typical metabolic graph of each group

The samples of each group were analyzed using UHPLC–Q/TOF–MS/MS in positive- and negative-ion modes, and typical TIC graphs were obtained (Figure S2). The figure shows some differences in metabolic profiles among the different groups. The results demonstrate the significant changes in the kinds and contents of metabolites in the serum from different groups, which indicate the importance of the metabolic spectrum analysis (Yin et al., 2018).

2. PCA score plot of each group

The PCA score plot of each group is shown in Figure 1. The figure reveals that the distance between the samples of the model (48 h) and control groups was relatively great, which indicated that the liver injury was severe at 48 h after model establishment. The samples in the different intervention groups were close to those in the control group at 48 h after model establishment. Therefore, 48 h after the model establishment was screened as the significant time point for liver injury and drug intervention for the following analysis. The PCA results reflect the occurrence of liver injury and the intervention effects of CASP and UASP to some extent (Mounet et al., 2007).

3.1.3 | Metabolite data analysis results of control and model groups

1. Multivariate statistical analysis

The detection data of UPLC–TOF–MS/MS of the control and model (48 h) groups were analyzed using PCA to investigate the metabolic changes in the liver injury model of layer chickens. The results showed that the two groups could achieve significant separation under positive- and negative-ion modes ($R^2X = 0.514$ and 0.609, respectively). The PCA score plot (Figure S3a) showed that the sample points of the control and model (48 h) groups were significantly separated, especially under the positive-ion mode. PLS-DA was used to further analyze the different metabolites between the two groups.

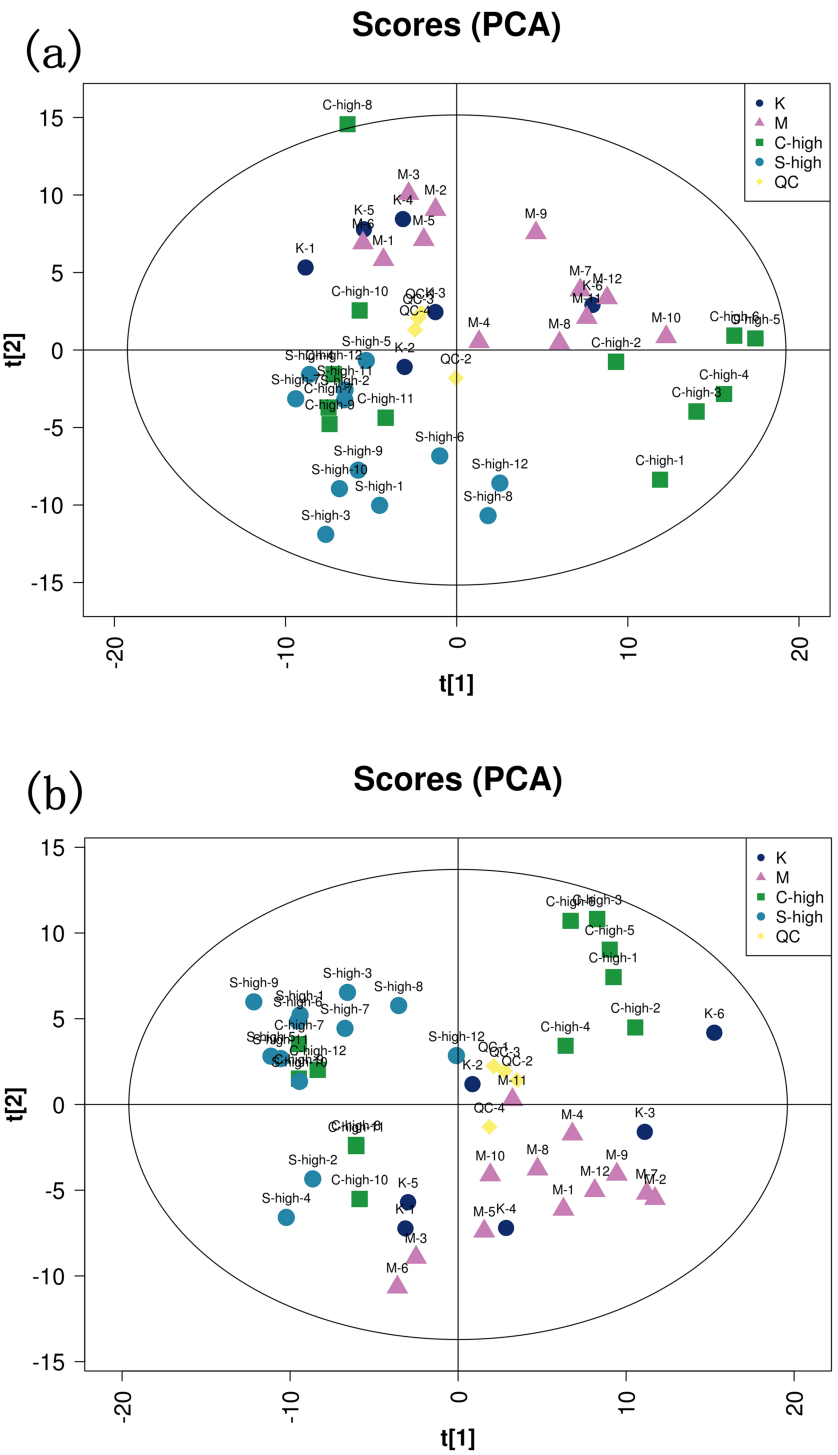

FIGURE 1 (a, b) Principal component analysis score plot of all samples (including quality control samples). (a) Positive-ion mode; (b) negative-ion mode. Note: K, control group; M, model group; C-high, high-dose intervention group of CASP; S-high, high-dose intervention group of the high-dose intervention group of UASP

The model evaluation parameters of the PLS-DA model between the control group and model group (R^2X, R^2Y, Q^2) under positive- and negative-ion modes were 0.319, 0.978, 0.523 and 0.255, 0.984, and 0.113, respectively. The results of the PLS-DA replacement test are presented in Figure S3b. Both figures revealed the reliability of the PLS-DA model. The sample points of the control and model (48 h) groups were completely separated under the positive- and negative-ion modes according to the PLS-DA analysis score plot (Figure S3c). Compared with the PLS-DA method, OPLS-DA can effectively reduce the complexity of the model and enhance its interpretation capability without reducing its prediction capability to maximize checking of the differences between the two groups and screening of the potential differential metabolites (Westerhuis et al., 2010). The model evaluation parameters of the OPLS-DA model between the control group and model group (R^2X, R^2Y, Q^2) under positive- and negative-ion modes were 0.449, 0.997, 0.583 and 0.38, 0.997, 0.45, respectively.

The OPLS-DA replacement test results are presented in Figure 2. Both tables reveal the reliability of the OPLS-DA model. The sample

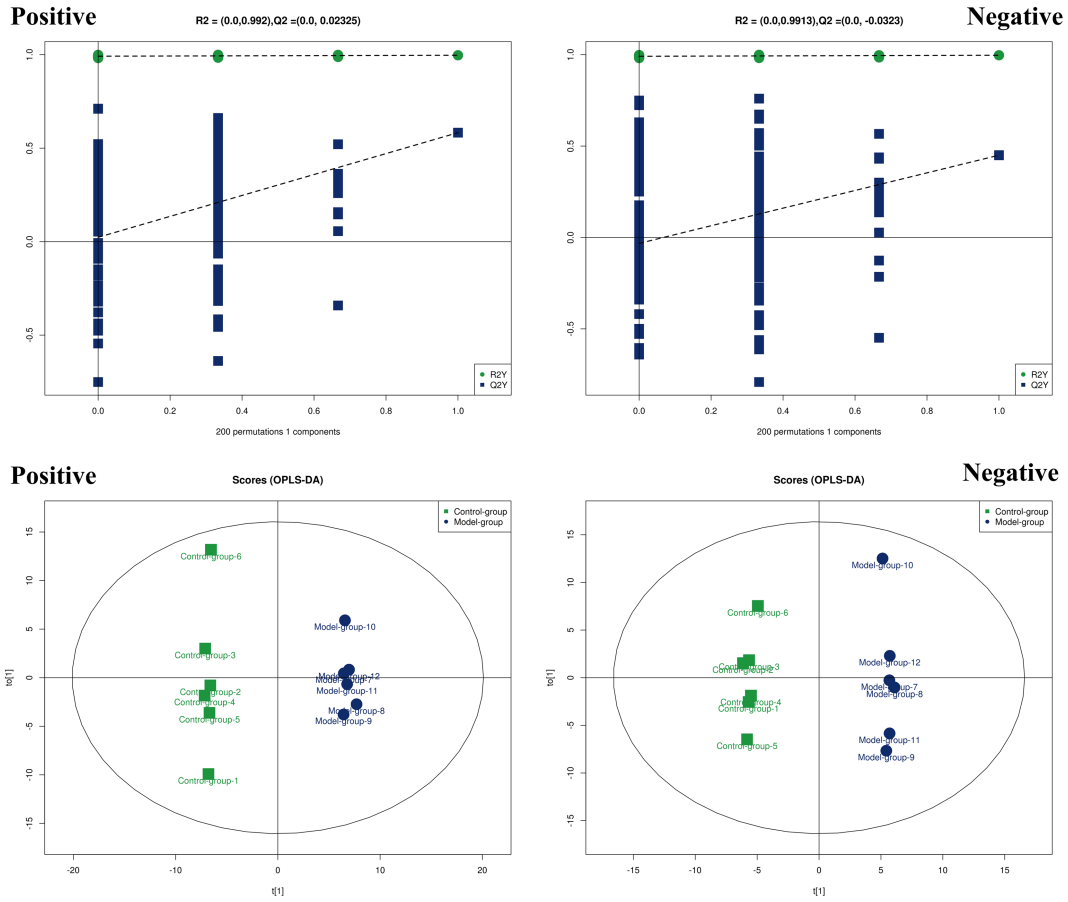

FIGURE 2 Orthogonal partial least squares discriminant analysis (OPLS-DA) replacement test (top) and score plot (bottom) of the control and model (48 h) groups in positive-ion mode and negative-ion mode

points of the control and model (48 h) groups were completely separated under the positive- and negative-ion modes according to the score plot of OPLS-DA (Figure 2). The above results further indicate that the liver injury model of layer chicken was successfully established. This method of judgment was frequently used in past studies (Bogdanovska et al., 2017; Xie et al., 2019; Yang, Li, et al., 2019). It was worth mentioning that the successful establishment of the liver injury model of layer chicken was also proved according to the detection results of recognized liver injury biochemical indicators of aspartic transaminase (AST) and alanine aminotransferase (ALT) before (He, 2019).

2. Screening, identification and bioinformatics analyses of different metabolites

The volcano map analysis results of the control and model (48 h) groups under positive- and negative-ion modes are shown in Figure 3a. The red dot marks in Figure 3a are the metabolites with FC > 1.5 and p-value < 0.05. The detected differential metabolites (VIP > 1.0) under the positive- and negative-ion modes are presented in Table 1. These metabolites were identified by accurate mass number matching (<25 ppm) and secondary spectrogram matching and searching the database of established standards of the laboratory. Hierarchical cluster analysis was used to verify the reliability of the differential metabolites in Table 1. The results showed the reasonability of the screened and identified differential metabolites under the positive- and negative-ion modes (Figure 3b). The KEGG pathway enrichment analysis of 54 selected differential metabolites was conducted using Fisher's exact test. The results revealed significant changes (Figure 3c, Rich factor > 0.05, p-value < 0.05) in 12 important metabolic pathways as follows: mTOR signaling pathway; alanine, aspartate and glutamate metabolism; glyoxylate and dicarboxylate metabolism; pyrimidine metabolism; aminoacyl-tRNA biosynthesis; lysine degradation; linoleic acid metabolism; pyruvate metabolism; citrate cycle (TCA cycle); ABC transporters; histidine metabolism; and valine, leucine, and isoleucine biosynthesis. Moreover, these pathways were involved in inflammation-related pathways, energy metabolism and amino acid metabolism disorder. The specific parameters are shown in Table 2. The results were consistent with the previous studies. Zhou B. G. found that the mTOR signaling pathway was closely related to liver injury (Zhou et al., 2017). Du X. W. also found that alanine, aspartate and glutamate metabolism was closely related to liver injury (Du et al., 2013). Lu X. Y. reported the close relationship of ABC transporters with liver injury (Lu et al., 2014).

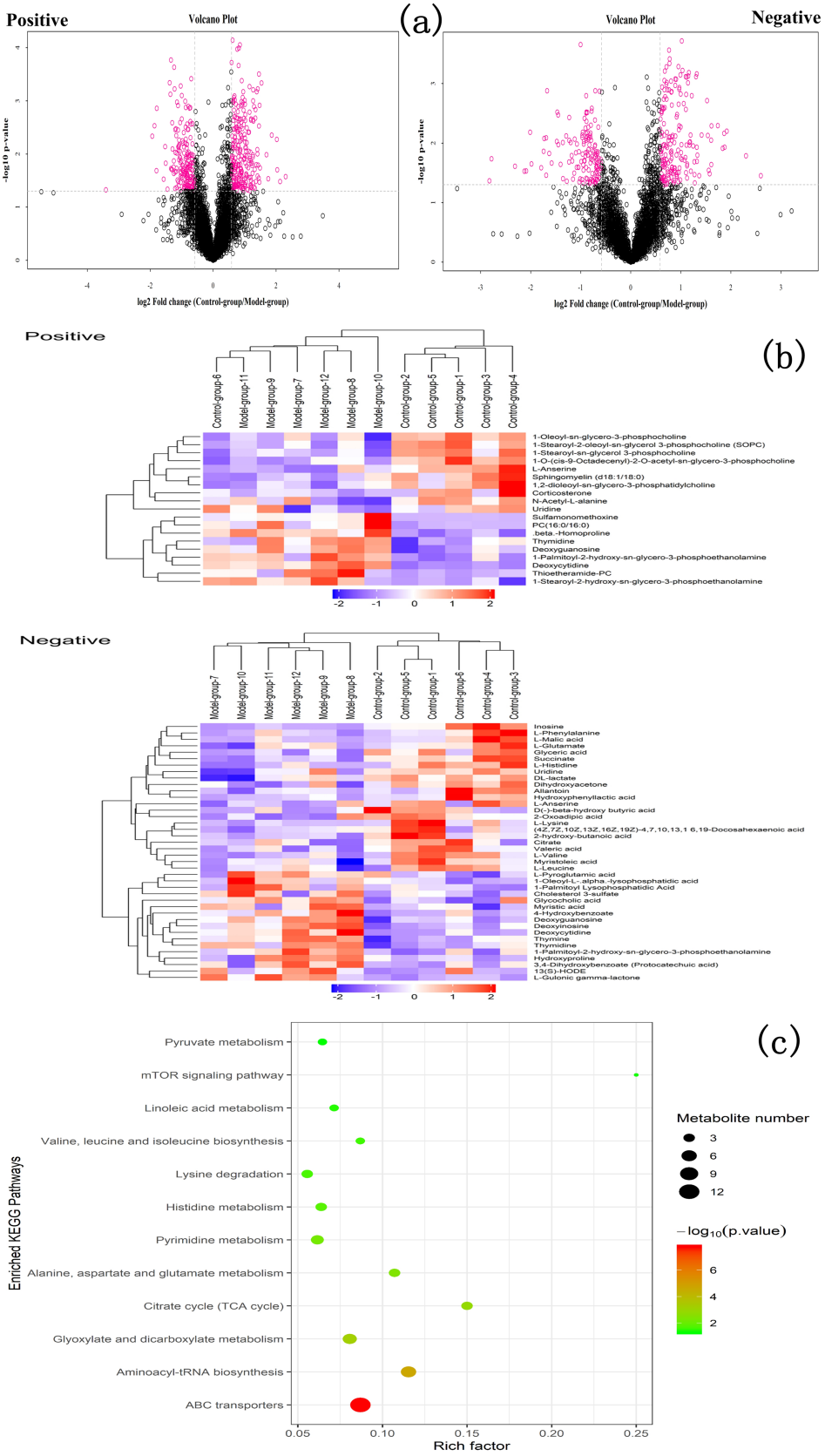

FIGURE 3 (a) Analysis results of voltano plot of the control and model (48 h) groups (left, positive-ion mode; right, negative-ion mode). (b) Hierarchical clustering results of differential metabolites of the control and model (48 h) groups (top, positive-ion mode; bottom, negative-ion mode). (c) Analysis results of KEGG pathway enrichment of differential metabolites in positive- and negative-ion modes between the control and model (48 h) groups

TABLE 1 Differential metabolites identified under positive- and negative-ion modes between the control and model groups

Ion mode	Description	VIP	Fold change	*p*-Value	*m/z*	Retention time
Positive	Deoxycytidine	1.6886	0.5397	0.001	228	422
	β-Homoproline	1.5464	0.5635	0.0027	130	737
	Deoxyguanosine	1.2213	0.6296	0.0107	268	467
	Thymidine	1.3375	0.562	0.019	243	177
	1-Stearoyl-2-oleoyl-sn-glycerol 3-phosphocholine (SOPC)	7.7395	1.6256	0.0194	811	304
	1-Palmitoyl-2-hydroxy-sn-glycero-3-phosphoethanolamine	3.4111	0.7949	0.0214	454	401
	L-Anserine	2.7737	1.5828	0.0323	241	830
	Thioetheramide-PC	10.283	0.4892	0.0343	759	104
	1-Stearoyl-2-hydroxy-sn-glycero-3-phosphoethanolamine	1.5805	0.8066	0.0382	482	410
	1-*O*-(*cis*-9-Octadecenyl)-2-*O*-acetyl-sn-glycero-3-phosphocholine	1.7271	1.6287	0.0404	573	374
	1-Stearoyl-sn-glycerol 3-phosphocholine	2.5603	1.5735	0.0434	568	376
	Sulfamonomethoxine	2.3057	0.0943	0.0472	281	69
	Sphingomyelin (d18:1/18:0)	1.4646	1.3577	0.0522	795	79
	Corticosterone	1.3249	2.6344	0.0534	347	66
	PC (16:0/16:0)	1.8605	0.4539	0.0591	735	167
	1-Oleoyl-sn-glycero-3-phosphocholine	7.439	1.4993	0.0617	544	379
	1,2-Dioleoyl-sn-glycero-3-phosphatidylcholine	1.8337	1.3935	0.069	769	80
	N-Acetyl-L-alanine	4.0021	1.1921	0.0702	132	697
	Uridine	2.093	1.2866	0.082	245	320
Negative	L-Gulonic γ-lactone	4.376	0.6483	0.0013	177	187.69
	Inosine	3.5872	2.8763	0.0019	249.1	227.78
	Succinate	6.3902	2.08	0.0022	117	707.37
	Thymidine	9.1087	0.5813	0.0029	241.1	161.26
	Glyceric acid	2.1779	1.5404	0.003	105	555.27
	Deoxyguanosine	1.328	0.5408	0.003	266.1	414.58
	Deoxycytidine	1.354	0.3658	0.0034	226.1	374.01
	Deoxyinosine	4.6727	0.5341	0.0056	251.1	324.69
	L-Histidine	2.0103	2.9048	0.0074	154.1	766.48
	L-Valine	2.3715	1.4107	0.0075	116.1	550.96
	Thymine	2.037	0.6743	0.0076	125	160.73
	Valeric acid	1.1638	1.5373	0.013	101.1	163.06
	2-Hydroxy-butanoic acid	2.8243	2.026	0.0188	103	341.53
	Dihydroxyacetone	2.1085	1.4504	0.0207	89.02	546.24
	DL-Lactate	8.3169	1.2321	0.0211	89.02	415.01
	2-Oxoadipic acid	2.1639	1.2969	0.0242	181	672.91
	1-Palmitoyl-2-hydroxy-sn-glycero-3-phosphoethanolamine	1.7205	0.7779	0.0262	452.3	359.25
	L-Lysine	3.1882	2.9423	0.0287	145.1	989.62
	Glycocholic acid	1.2277	0.7798	0.0322	464.3	313.73
	4-Hydroxybenzoate	1.3195	0.586	0.0325	137	56.054
	Uridine	3.9682	1.3286	0.0378	243.1	287.97
	Myristoleic acid	2.0384	1.259	0.0385	225.2	73.593
	Myristic acid	2.1976	0.8663	0.043	227.2	73.647
	Allantoin	1.1806	1.4486	0.0437	139	515.72

TABLE 1 (Continued)

Ion mode	Description	VIP	Fold change	*p*-Value	*m/z*	Retention time
	L-Anserine	1.237	1.5085	0.0507	239.1	770.96
	1-Oleoyl-L-α-lysophosphatidic acid	1.6288	0.5103	0.0535	435.3	431.32
	Hydroxyphenyllactic acid	1.278	1.7564	0.0538	181.1	337.48
	1-Palmitoyl lysophosphatidic acid	1.825	0.6059	0.0543	409.2	438.58
	L-Malic acid	3.2362	3.2589	0.0557	133	772.06
	D(−)-β-Hydroxy butyric acid	3.1044	1.8471	0.0568	103	431.75
	Cholesterol 3-sulfate	2.1949	0.7295	0.0571	465.3	37.751
	L-Pyroglutamic acid	3.6706	0.848	0.0657	128	545.02
	(4Z,7Z,10Z,13Z,16Z,19Z)-4,7,10,13,16,19-Docosahexaenoic acid	11.672	1.3681	0.0724	327.2	67.743
	3,4-Dihydroxybenzoate (protocatechuic acid)	2.77	0.5684	0.0792	153	46.793
	L-Phenylalanine	1.2006	1.2063	0.0814	164.1	498.92
	L-Glutamate	2.8212	1.2056	0.084	146	727.4
	Hydroxyproline	2.0084	0.7123	0.086	130.1	637.09
	13(*S*)-HODE	2.4346	0.7522	0.0951	295.2	75.439
	L-Leucine	2.7297	1.1552	0.0976	130.1	500.92
	Citrate	2.2292	1.6808	0.0987	191	994.5

VIP, Variable importance in projection.

TABLE 2 Enrichment analysis of KEGG pathway of different metabolites in the positive- and negative-ion mode between the control and the model groups

Map name	Test	TestAll	Ref	RefAll	Test_per	Ref_per	*p*-Value	FDR	Rich factor
ABC transporters	12	36	138	3,116	33.33333333	4.428754814	1.7784×10^{-8}	9.06986×10^{-7}	0.086956522
Aminoacyl-tRNA biosynthesis	6	36	52	3,116	16.66666667	1.668806162	2.13738×10^{-5}	0.000545031	0.115384615
Glyoxylate and dicarboxylate metabolism	5	36	62	3,116	13.88888889	1.989730424	0.000621342	0.01056282	0.080645161
Citrate cycle (TCA cycle)	3	36	20	3,116	8.333333333	0.641848524	0.001411178	0.017992525	0.15
Alanine, aspartate and glutamate metabolism	3	36	28	3,116	8.333333333	0.898587933	0.003805877	0.038819948	0.107142857
Pyrimidine metabolism	4	36	65	3,116	11.11111111	2.086007702	0.006155139	0.052318682	0.061538462
Histidine metabolism	3	36	47	3,116	8.333333333	1.508344031	0.016212285	0.118118076	0.063829787
Lysine degradation	3	36	54	3,116	8.333333333	1.732991014	0.023471518	0.149630924	0.055555556
Valine, leucine and isoleucine biosynthesis	2	36	23	3,116	5.555555556	0.738125802	0.028201314	0.159807447	0.086956522
Linoleic acid metabolism	2	36	28	3,116	5.555555556	0.898587933	0.040647482	0.20333247	0.071428571
mTOR signaling pathway	1	36	4	3,116	2.777777778	0.128369705	0.045439876	0.20333247	0.25
Pyruvate metabolism	2	36	31	3,116	5.555555556	0.994865212	0.048939392	0.20333247	0.064516129

3.1.4 | Metabolite data analysis results of CASPG and the model group (48 h)

1. Multivariate statistical analysis

The detection data of UPLC–TOF–MS/MS of CASPG and the model group (48 h) were analyzed by PCA to investigate the effect of CASP on the metabolic changes in the liver injury model of layer chickens. The results showed that the two groups could achieve significant separation under positive- and negative-ion modes ($R^2X = 0.559$ and 0.549, respectively). The PCA score plot (Figure S4a) showed that the sample points of CASPG and the model group (48 h) were significantly separated, especially under the positive-ion mode. The serum metabolism spectrum changed significantly, which indicated that CASP had a significant intervention effect on the liver injury model of layer chickens caused by CS combined with LPS. PLS-DA was used further to analyze the different metabolites between the two groups. The model evaluation parameters of

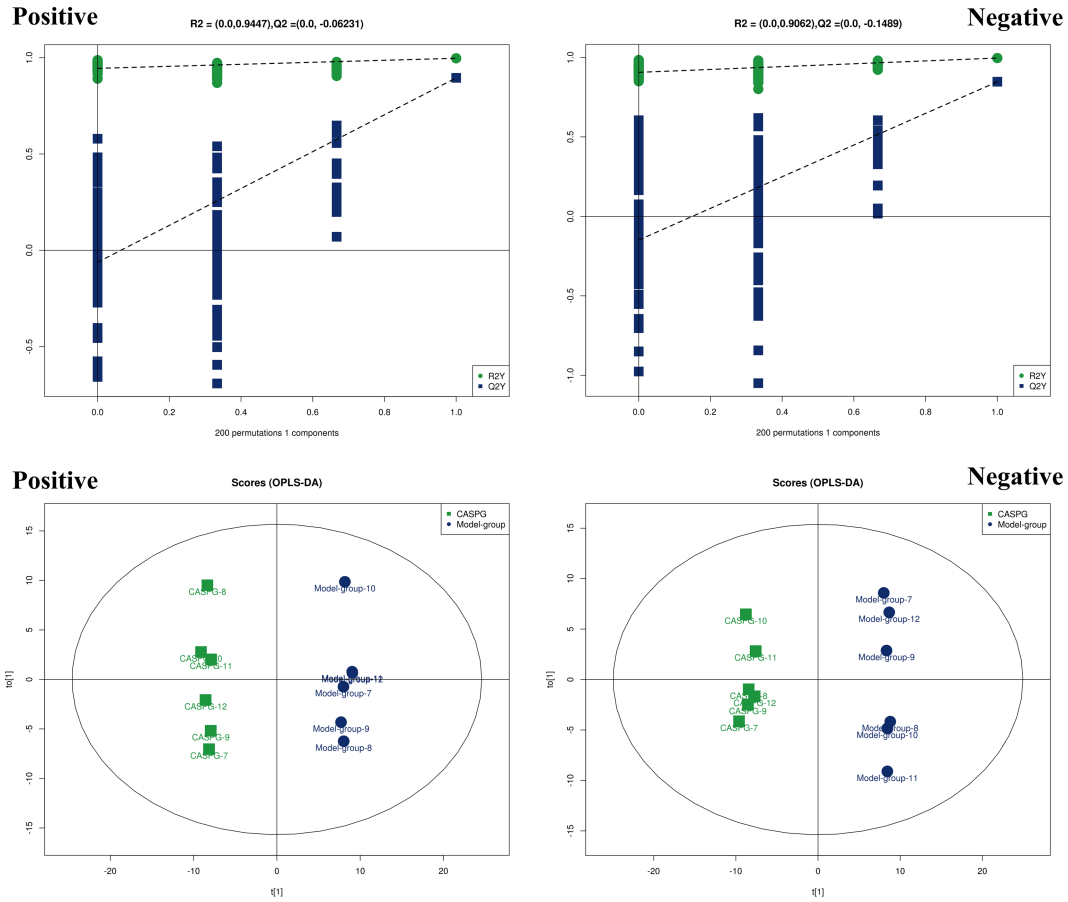

FIGURE 4 OPLS-DA replacement test (top) and score plot (bottom) between the high-dose intervention group of polysaccharides from charred *Angelica sinensis*(CASPG) and model groups in positive-ion mode and negative-ion mode

the PLS-DA model between the control group and the model group (R^2X, R^2Y, Q^2) under positive- and negative-ion modes were 0.357, 0.997, 0.887 and 0.376, 0.996, and 0.876, respectively. The results of the PLS-DA replacement test are presented in Figure S4b. Both figures revealed the reliability of the PLS-DA model. The sample points of CASPG and the model group (48 h) were wholly separated under the positive- and negative-ion modes according to the PLS-DA analysis score plot (Figure S4c). The model evaluation parameters of the OPLS-DA model between the control group and model group (R^2X, R^2Y, Q^2) under positive- and negative-ion modes were 0.413, 0.994, 0.93 and 0.385, 0.994, 0.894, respectively. The OPLS-DA replacement test results are shown in Figure 4a. The sample points of CASPG and the model group (48 h) were utterly separated under the positive- and negative-ion modes according to the score plot of OPLS-DA (Figure 4b). In conclusion, CASP had a significant effect on the liver injury model of layer chickens.

2. Screening, identification and bioinformatics analysis of different metabolites

The volcano map analysis results of CASPG and the model group (48 h) under positive- and negative-ion modes are shown in Figure 5a. The red dot marks in Figure 5a are the metabolites with fold change (FC) > 1.5 and p-value < 0.05. The detected differential metabolites (VIP > 1.0) under the positive- and negative-ion modes are presented in Table 3. These metabolites were identified by accurate mass number matching (<25 ppm) and secondary spectrogram matching and searching the database of established standards by the laboratory. Hierarchical cluster analysis was used to verify the reliability of the differential metabolites in Table 3. The results showed the reasonability of the screened and identified differential metabolites under positive- and negative-ion modes (Figure 5b). The KEGG pathway enrichment analysis of 82 selected differential metabolites was conducted using Fisher's exact test. The results revealed significant changes (Figure 5c, Rich factor > 0.05, p-value < 0.05) in 16 important metabolic pathways as follows: arachidonic acid metabolism; mTOR signaling pathway; ABC transporters; aminoacyl-tRNA biosynthesis; valine, leucine and isoleucine biosynthesis; arginine biosynthesis; pyrimidine metabolism; linoleic acid metabolism; β-alanine metabolism; valine, leucine and isoleucine degradation; pantothenate and CoA biosynthesis; alanine, aspartate and glutamate metabolism; purine metabolism; vascular smooth muscle contraction; biosynthesis of unsaturated fatty acids; and histidine metabolism. Moreover, these pathways were

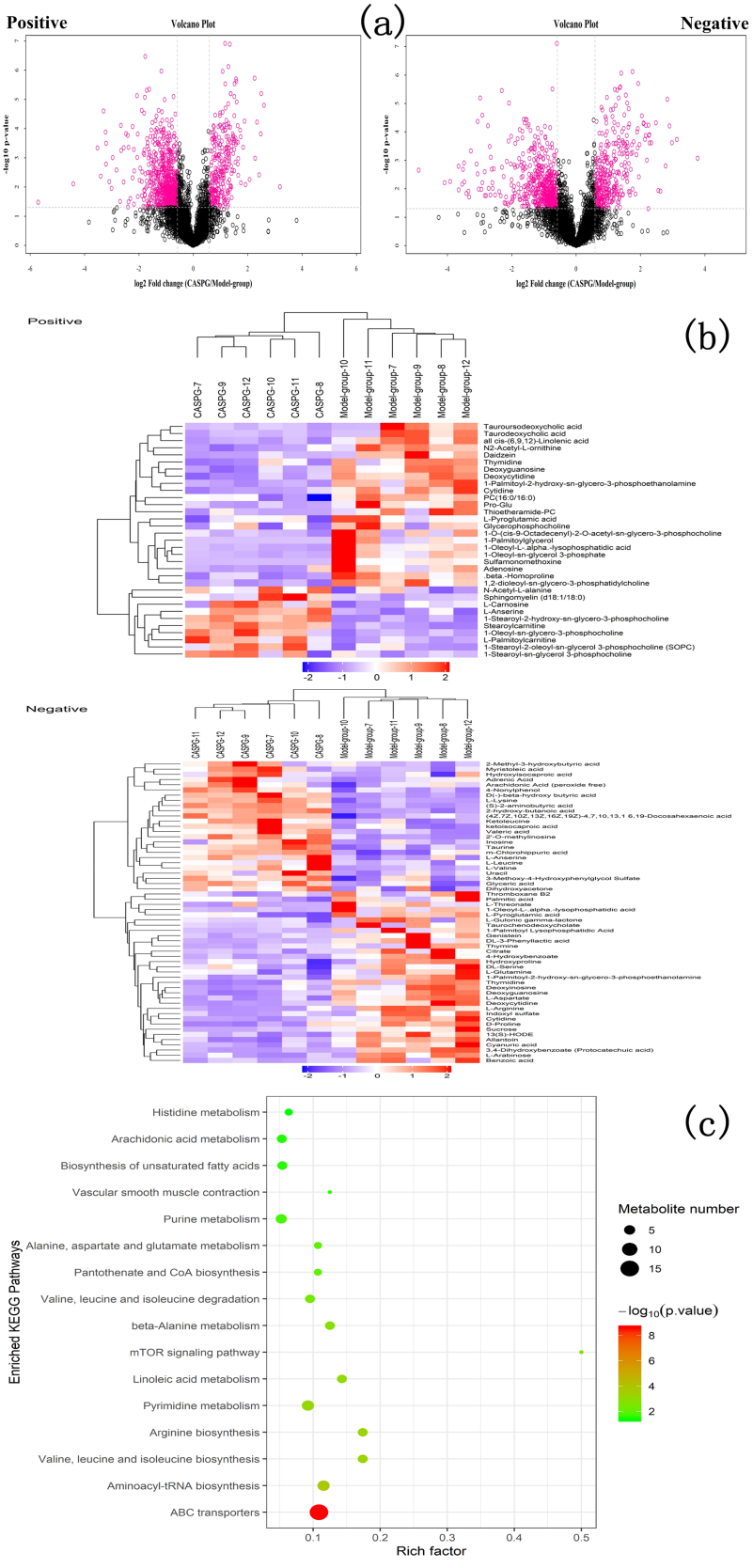

FIGURE 5 (a) Analysis results of voltano plot between CASPG and model-group (left, positive-ion mode; right, negative-ion mode). (b) Hierarchical clustering results of differential metabolites between CASPG and model-group (top, positive-ion mode; bottom, negative-ion mode). (c) Analysis results of KEGG pathway enrichment of differential metabolites in positive- and negative-ion mode between CASPG and the model group

involved in the related inflammation-related pathways, energy metabolism, amino acid metabolism, unsaturated fatty acid biosynthesis pathway and so on. The specific parameters are shown in Table 4. The results were consistent with the previous studies. Wang R. X. reported the close relationship of ABC transporters with liver injury (Wang et al., 2011).

TABLE 3 Differential metabolites identified under positive- and negative-ion modes between CASPG and the model group

Ion mode	Description	VIP	Fold change	*p*-Value	*m/z*	Retention time
Positive	Stearoylcarnitine	1.8302	2.993	2×10^{-6}	428.4	336
	1-Stearoyl-2-hydroxy-sn-glycero-3-phosphocholine	1.42445	2.253	3×10^{-6}	568.3	396
	Deoxycytidine	1.60483	0.432	7×10^{-5}	228.1	422
	1,2-Dioleoyl-sn-glycero-3-phosphatidylcholine	3.57275	0.607	0.0002	786.6	282
	L-Anserine	4.22777	2.066	0.0003	241.1	830
	1-Palmitoyl-2-hydroxy-sn-glycero-3-phosphoethanolamine	3.29274	0.706	0.0003	454.3	401
	All *cis*-(6,9,12)-linolenic acid	2.37023	0.426	0.0005	279.2	74.4
	Deoxyguanosine	1.13429	0.552	0.0005	268.1	467
	β-Homoproline	1.38764	0.55	0.0006	130.1	737
	Cytidine	1.82129	0.28	0.0007	244.1	487
	N2-Acetyl-L-ornithine	5.26574	0.654	0.001	175.1	1,029
	1-Oleoyl-sn-glycero-3-phosphocholine	2.47285	2.487	0.0011	544.3	412
	L-Palmitoylcarnitine	1.11905	2.843	0.0028	400.3	344
	PC (16:0/16:0)	1.71058	0.661	0.0052	756.6	314
	1-Oleoyl-L-α-lysophosphatidic acid	1.22426	0.366	0.0074	419.3	504
	Thymidine	1.24548	0.466	0.0081	243.1	177
	Pro-Glu	1.26081	0.416	0.0089	286.1	838
	Daidzein	2.57037	0.306	0.0094	255.1	37.2
	1-Stearoyl-2-oleoyl-sn-glycerol 3-phosphocholine (SOPC)	6.14051	2.022	0.0104	810.6	268
	1-Oleoyl-sn-glycerol 3-phosphate	1.01308	0.357	0.0108	437.3	504
	Taurodeoxycholic acid	1.47788	0.568	0.0122	517.3	77.2
	Thioetheramide-PC	9.70997	0.394	0.0177	758.6	104
	Adenosine	1.8419	0.425	0.0202	268.1	345
	1-O-(*cis*-9-Octadecenyl)-2-O-acetyl-sn-glycero-3-phosphocholine	1.67216	0.705	0.0267	550.4	375
	L-Carnosine	1.74089	1.485	0.0273	227.1	841
	Tauroursodeoxycholic acid	1.08343	0.585	0.029	482.3	76.5
	Sphingomyelin (d18:1/18:0)	1.47525	1.769	0.0322	794.6	139
	N-Acetyl-L-alanine	5.07012	1.284	0.0324	132.1	697
	Sulfamonomethoxine	2.35409	0.019	0.0332	281.1	69.3
	1-Palmitoylglycerol	1.57715	0.133	0.0629	313.3	72.6
	L-Pyroglutamic acid	1.41825	0.671	0.0712	276.1	852
	Glycerophosphocholine	2.96464	0.71	0.0808	258.1	780
	1-Stearoyl-sn-glycerol 3-phosphocholine	2.2424	1.219	0.0933	524.4	413
Negative	2-Hydroxy-butanoic acid	3.755	3.3708	8×10^{-7}	103.04	341.5
	(*S*)-2-Aminobutyric acid	1.11	3.8034	2×10^{-6}	102.06	595.8
	L-Lysine	2.922	2.9978	1×10^{-5}	145.1	989.6
	D(−)β-Hydroxy butyric acid	6.686	5.5713	5×10^{-5}	103.04	431.8
	Allantoin	2.981	0.4382	0.0002	157.04	324.5
	2′-O-Methylinosine	1.116	2.4976	0.0002	281.09	347.2
	(4Z,7Z,10Z,13Z,16Z,19Z)-4,7,10,13,16,19-Docosahexaenoic acid	11.71	1.4741	0.0003	327.23	67.74
	Taurine	6.149	2.0264	0.0003	124.01	537.1

TABLE 3 (Continued)

Ion mode	Description	VIP	Fold change	*p*-Value	*m/z*	Retention time
	L-Aspartate	1.067	0.596	0.0004	132.03	742.9
	Deoxyguanosine	1.001	0.5126	0.0006	266.09	414.6
	Thymidine	7.143	0.5444	0.0008	241.08	161.3
	4-Nonylphenol	2.166	1.6719	0.001	219.17	51.61
	D-Proline	2.532	0.6822	0.001	114.06	573.5
	Deoxycytidine	1.046	0.3084	0.0012	226.08	374
	m-Chlorohippuric acid	3.721	1.276	0.0013	213.02	252
	3,4-Dihydroxybenzoate (protocatechuic acid)	3.52	0.1172	0.0014	153.02	46.79
	Cytidine	1.293	0.2683	0.0017	242.08	437
	Glyceric acid	1.555	1.4094	0.0018	105.02	555.3
	Ketoisocaproic acid	7.839	1.54	0.0023	129.06	69.6
	13(*S*)-HODE	2.632	0.5844	0.0027	295.23	75.44
	1-Palmitoyl-2-hydroxy-sn-glycero-3-phosphoethanolamine	1.339	0.7343	0.0031	452.28	359.2
	L-Arginine	1.073	0.6828	0.0039	173.1	972.8
	Valeric acid	1.44	2.0331	0.004	101.06	163.1
	Cyanuric acid	1.157	0.3858	0.0041	145.04	160.5
	4-Hydroxybenzoate	1.197	0.4472	0.0041	137.02	56.05
	Deoxyinosine	3.203	0.5511	0.0044	251.08	324.7
	L-Valine	2.71	1.848	0.0045	116.07	551
	Ketoleucine	6.871	1.6686	0.0051	129.06	95.12
	L-Arabinose	1.904	0.5055	0.0067	149.04	555.8
	DL-3-Phenyllactic acid	3.252	0.2476	0.0074	165.05	152.2
	L-Anserine	1.278	1.7396	0.0086	239.11	771
	L-Pyroglutamic acid	4.621	0.7233	0.009	128.03	545
	3-Methoxy-4-hydroxyphenylglycol sulfate	2.237	1.483	0.0116	263.02	59.42
	Benzoic acid	2.419	0.4198	0.0144	121.03	177.1
	1-Oleoyl-L-α-lysophosphatidic acid	1.528	0.4018	0.016	435.25	431.3
	Myristoleic acid	2.788	1.6514	0.0164	225.19	73.59
	Indoxyl sulfate	2.522	0.2537	0.0194	212	40.3
	Inosine	1.605	1.6066	0.0254	249.06	227.8
	Hydroxyproline	1.898	0.5514	0.0259	130.05	637.1
	1-Palmitoyl lysophosphatidic acid	2.73	0.2527	0.0269	409.23	453
	L-Glutamine	2.87	0.6623	0.0276	145.06	686.3
	Uracil	4.884	2.1394	0.0291	111.02	145.2
	Citrate	1.081	0.587	0.0297	191.02	1,015
	Sucrose	1.187	0.2134	0.0307	341.11	677.6
	Genistein	1.455	0.423	0.0407	269.04	36.09
	Thymine	2.126	0.5325	0.0421	125.04	177.1
	2-Methyl-3-hydroxybutyric acid	2.021	1.7602	0.0467	117.06	244.3
	Dihydroxyacetone	1.519	1.3423	0.0504	89.024	546.2
	DL-Serine	1.221	0.6943	0.0518	104.03	691.1
	L-Gulonic γ-lactone	1.541	0.8175	0.056	177.04	187.7
	Thromboxane B2	1.562	0.5132	0.0565	369.23	260.6

(Continues)

TABLE 3 (Continued)

Ion mode	Description	VIP	Fold change	*p*-Value	*m/z*	Retention time
	L-Threonate	1.571	0.6076	0.0573	135.03	578
	Arachidonic acid (peroxide free)	12.83	1.2512	0.0678	303.23	67.65
	L-Leucine	3.366	1.3353	0.0698	130.09	500.9
	Taurochenodeoxycholate	4.015	0.4429	0.0724	498.29	279.6
	Hydroxyisocaproic acid	4.517	1.3557	0.0757	131.07	207.3
	Adrenic acid	5.623	1.3017	0.0832	331.26	65.96
	Palmitic acid	1.909	0.7398	0.0874	255.23	188

CASPG, High-dose intervention group of polysaccharides from charred *Angelica sinensis*.

TABLE 4 Enrichment analysis of KEGG pathway of different metabolites in the positive- and negative-ion modes between CASPG and the model group

Map name	Test	TestAll	Ref	RefAll	Test_per	Ref_per	*p*-Value	FDR	Rich factor
ABC transporters	15	52	138	3,116	28.84615385	4.428754814	2.55335×10^{-9}	1.27668×10^{-7}	0.108695652
Aminoacyl-tRNA biosynthesis	6	52	52	3,116	11.53846154	1.668806162	0.000182154	0.004553848	0.115384615
Valine, leucine and isoleucine biosynthesis	4	52	23	3,116	7.692307692	0.738125802	0.000483246	0.006040572	0.173913043
Arginine biosynthesis	4	52	23	3,116	7.692307692	0.738125802	0.000483246	0.006040572	0.173913043
Pyrimidine metabolism	6	52	65	3,116	11.53846154	2.086007702	0.000626141	0.006261407	0.092307692
Linoleic acid metabolism	4	52	28	3,116	7.692307692	0.898587933	0.001050505	0.008754208	0.142857143
mTOR signaling pathway	2	52	4	3,116	3.846153846	0.128369705	0.001604452	0.010976374	0.5
β-Alanine metabolism	4	52	32	3,116	7.692307692	1.026957638	0.00175622	0.010976374	0.125
Valine, leucine and isoleucine degradation	4	52	42	3,116	7.692307692	1.3478819	0.004833783	0.026854347	0.095238095
Pantothenate and CoA biosynthesis	3	52	28	3,116	5.769230769	0.898587933	0.010701708	0.048644125	0.107142857
Alanine, aspartate and glutamate metabolism	3	52	28	3,116	5.769230769	0.898587933	0.010701708	0.048644125	0.107142857
Purine metabolism	5	52	95	3,116	9.615384615	3.048780488	0.019863668	0.082765285	0.052631579
Vascular smooth muscle contraction	2	52	16	3,116	3.846153846	0.513478819	0.028232409	0.108586189	0.125
Biosynthesis of unsaturated fatty acids	4	52	74	3,116	7.692307692	2.374839538	0.033620138	0.116953372	0.054054054
Arachidonic acid metabolism	4	52	75	3,116	7.692307692	2.406931964	0.035086012	0.116953372	0.053333333
Histidine metabolism	3	52	47	3,116	5.769230769	1.508344031	0.042463719	0.13269912	0.063829787

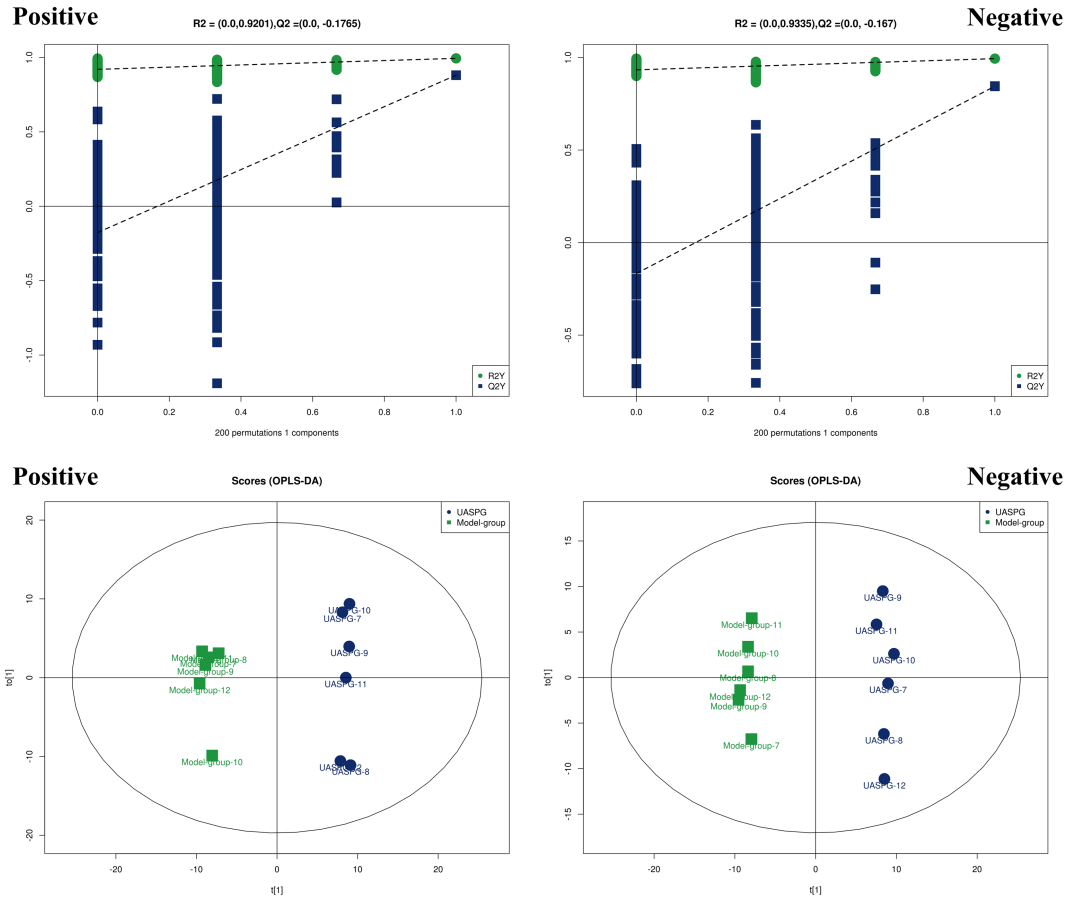

FIGURE 6 OPLS-DA replacement test (top) and score plot (bottom) between UASPG and model-group in positive-ion mode and negative-ion mode

3.1.5 | The metabolite data analysis results of UASPG and the model group (48 h)

1. Multivariate statistical analysis

The detection data of UPLC–TOF–MS/MS of UASPG and the model group (48 h) were analyzed by PCA to investigate the effect of UASP on the metabolic changes in the liver injury model of layer chickens. The results showed that the two groups could achieve significant separation under positive- and negative-ion modes ($R^2X = 0.551$ and 0.538, respectively). The PCA score plot (Figure S5) showed that the sample points of UASPG and the model group (48 h) were significantly separated, especially under the positive-ion mode. The serum metabolism spectrum changed significantly, which indicated that UASP had an intervention effect on the liver injury model of layer chickens caused by CS combined with LPS. PLS-DA was used to further analyze the different metabolites between the two groups. The model evaluation parameters of the PLS-DA model between the control group and model group (R^2X, R^2Y, Q^2) under positive- and negative-ion modes were 0.413, 0.994, 0.93 and 0.385, 0.994, and 0.894, respectively. The results of the PLS-DA replacement test are presented in Figure S5b. Both figures revealed the reliability of the PLS-DA model. The sample points of UASPG and the model group (48 h) were wholly separated under the positive- and negative-ion modes according to the PLS-DA analysis score plot (Figure S5c). The model evaluation parameters of the OPLS-DA model between the control group and model group (R^2X, R^2Y, Q^2) under positive- and negative-ion modes were 0.413, 0.994, 0.93 and 0.385, 0.994, and 0.894, respectively. The OPLS-DA replacement test results are shown in Figure 6a. Both tables reveal the reliability of the OPLS-DA model. The sample points of UASPG and the model group (48 h) were separated under the positive- and negative-ion modes according to the score plot of OPLS-DA analysis (Figure 6b). In conclusion, UASP had a significant effect on the liver injury model of layer chickens.

2. Screening, identification and bioinformatics analyses of different metabolites

The volcano map analysis results of UASPG and the model group (48 h) under the positive- and negative-ion mode are shown in Figure 7a. The red dot marks in Figure 7a are the metabolites with FC > 1.5 and p-value < 0.05. The detected differential metabolites (VIP > 1.0) under the positive- and negative-ion modes are presented in Table 5. These metabolites were identified by accurate mass

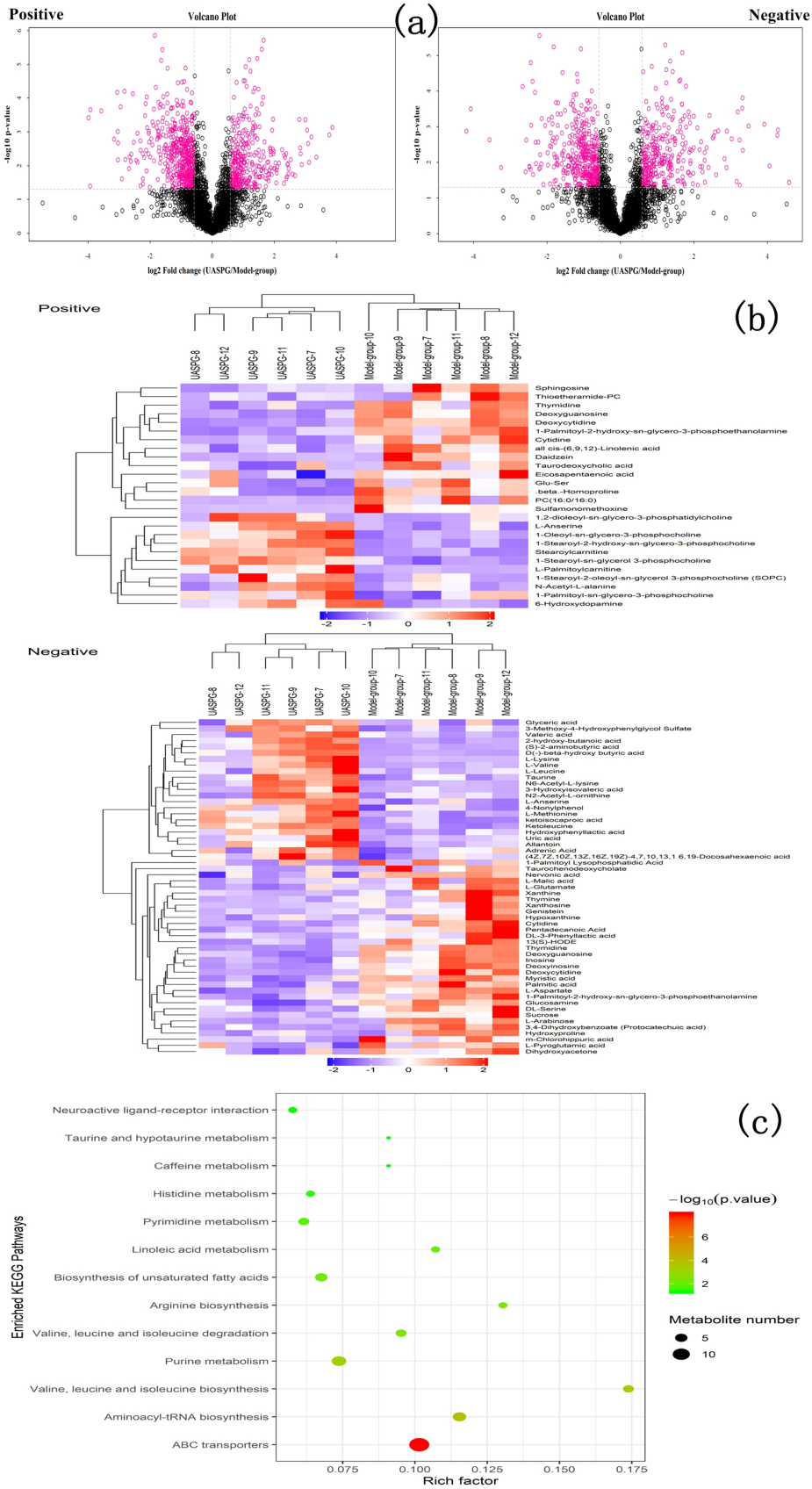

FIGURE 7 (a) Analysis results of voltano plot between UASPG and model-group (left, positive-ion mode; right: negative-ion mode); hierarchical clustering results of differential metabolites between UASPG and model-group (top, positive-ion mode; bottom, negative-ion mode). (c) Analysis results of KEGG pathway enrichment of differential metabolites between UASPG and model group in positive- and negative-ion mode

TABLE 5 Differential metabolites identified under the positive- and negative-ion modes between UASPG and the model group

Ion mode	Description	VIP	Fold change	*p*-Value	*m/z*	Retention time
Positive	Stearoylcarnitine	1.6434	3.153	2×10^{-6}	428.4	336.3
	Deoxycytidine	1.739	0.328	4×10^{-6}	228.1	421.5
	1-Stearoyl-sn-glycerol 3-phosphocholine	3.1402	1.441	2×10^{-5}	524.4	413.3
	1-Stearoyl-2-hydroxy-sn-glycero-3-phosphocholine	1.1455	2.154	5×10^{-5}	568.3	396.1
	Deoxyguanosine	1.2533	0.505	2×10^{-4}	268.1	466.6
	1-Palmitoyl-2-hydroxy-sn-glycero-3-phosphoethanolamine	3.5697	0.707	7×10^{-4}	454.3	401.4
	Cytidine	1.773	0.29	7×10^{-4}	244.1	486.8
	1-Oleoyl-sn-glycero-3-phosphocholine	2.1059	2.443	9×10^{-4}	544.3	412.1
	L-Anserine	3.3521	1.981	0.001	241.1	830.1
	Thymidine	1.3998	0.422	0.003	243.1	176.6
	β-Homoproline	1.4155	0.553	0.004	130.1	736.9
	All *cis*-(6,9,12)-linolenic acid	2.0274	0.562	0.006	279.2	74.43
	L-Palmitoylcarnitine	1.7052	7.371	0.009	400.3	344.5
	PC (16:0/16:0)	1.9777	0.365	0.013	733.6	161.3
	Daidzein	2.4971	0.379	0.015	255.1	37.17
	Sphingosine	1.4749	0.534	0.02	300.3	95.4
	Glu–Ser	1.0618	0.63	0.038	235.1	851.3
	Sulfamonomethoxine	2.0498	0.066	0.041	281.1	69.27
	1,2-Dioleoyl-sn-glycero-3-phosphatidylcholine	3.3645	1.696	0.055	786.6	187.5
	Taurodeoxycholic acid	1.376	0.614	0.066	517.3	77.19
	1-Stearoyl-2-oleoyl-sn-glycerol 3-phosphocholine (SOPC)	4.8404	1.82	0.067	810.6	267.8
	N-Acetyl-L-alanine	5.3612	1.429	0.068	132.1	697.2
	1-Palmitoyl-sn-glycero-3-phosphocholine	2.1746	1.122	0.085	496.3	406.7
	Thioetheramide-PC	7.0698	0.603	0.087	758.6	103.9
	Eicosapentaenoic acid	1.0108	0.804	0.088	303.2	74.3
	6-Hydroxydopamine	1.1654	1.381	0.099	170.1	830.4
Negative	Ketoleucine	9.58735	2.3695	2×10^{-5}	129.1	95.12
	Thymidine	8.28507	0.4444	5×10^{-5}	241.1	161.3
	Ketoisocaproic acid	9.96477	1.9479	8×10^{-5}	129.1	69.6
	Deoxyguanosine	1.15203	0.4074	0.0002	266.1	414.6
	2-Hydroxy-butanoic acid	3.80767	3.9797	0.0005	103	341.5
	Palmitic acid	13.9938	0.7582	0.0005	255.2	72.39
	Deoxycytidine	1.07962	0.2582	0.0006	226.1	374
	L-Aspartate	1.14925	0.5274	0.0007	132	742.9
	D(−)-β-Hydroxy butyric acid	9.28862	11.223	0.0009	103	431.8
	Deoxyinosine	3.87202	0.4307	0.001	251.1	324.7
	Glucosamine	1.06938	0.5528	0.0013	238.1	586.6
	Cytidine	1.29636	0.2686	0.0015	242.1	437
	(S)-2-Aminobutyric acid	1.31992	5.818	0.0018	102.1	595.8
	L-Arabinose	2.1141	0.4245	0.0019	149	555.8
	Nervonic acid	1.48816	0.6564	0.002	365.3	64.48
	Inosine	1.20864	0.4876	0.0021	289.1	324.7
	Myristic acid	2.64044	0.7373	0.0021	227.2	73.65

(Continues)

TABLE 5 (Continued)

Ion mode	Description	VIP	Fold change	*p*-Value	*m/z*	Retention time
	L-Anserine	1.3771	1.8226	0.0026	239.1	771
	1-Palmitoyl-2-hydroxy-sn-glycero-3-phosphoethanolamine	1.42237	0.7298	0.0031	452.3	359.2
	L-Methionine	1.12851	1.8122	0.0032	148	518.9
	13(*S*)-HODE	2.44328	0.6086	0.0033	295.2	75.44
	DL-Serine	1.79764	0.5434	0.0038	104	691.1
	Pentadecanoic acid	1.58801	0.6715	0.0044	241.2	73.02
	3-Methoxy-4-hydroxyphenylglycol sulfate	2.86509	1.9558	0.0052	263	59.42
	3,4-Dihydroxybenzoate (protocatechuic acid)	3.01098	0.253	0.0054	153	46.79
	Hydroxyphenyllactic acid	1.11295	1.832	0.0057	181.1	337.5
	L-Valine	3.44248	2.4665	0.0067	116.1	551
	N6-Acetyl-L-lysine	1.08458	7.1064	0.0079	187.1	725.4
	4-Nonylphenol	1.6086	1.4271	0.0083	219.2	51.61
	Taurine	4.7478	1.7333	0.0107	124	537.1
	L-Pyroglutamic acid	3.97679	0.7517	0.014	128	545
	L-Glutamate	2.22497	0.7296	0.0143	146	727.4
	Allantoin	1.2486	1.753	0.0145	139	515.7
	Dihydroxyacetone	1.56447	0.8112	0.0154	89.02	560.6
	m-Chlorohippuric acid	1.51657	0.6881	0.022	213	188
	L-Lysine	3.907	6.0787	0.0223	145.1	989.6
	(4Z,7Z,10Z,13Z,16Z,19Z)-4,7,10,13,16,19-Docosahexaenoic acid	8.89914	1.3499	0.023	327.2	67.74
	Xanthine	2.20076	0.6468	0.0257	151	385.7
	Thymine	2.48489	0.4814	0.0274	125	177.1
	3-Hydroxyisovaleric acid	1.2982	3.152	0.0348	117.1	365.1
	Valeric acid	1.26689	1.7076	0.0365	101.1	182.7
	Hydroxyproline	1.76986	0.6301	0.0386	130.1	637.1
	Sucrose	1.09691	0.2647	0.04	341.1	677.6
	DL-3-Phenyllactic acid	2.19293	0.3724	0.0444	165.1	187.5
	Hypoxanthine	6.49232	0.6304	0.0487	135	301.1
	Xanthosine	1.62669	0.2797	0.0587	283.1	567.9
	Uric acid	2.2368	3.8705	0.0638	167	593.7
	Glyceric acid	1.00797	1.2465	0.0712	105	555.3
	Genistein	1.28401	0.5056	0.0714	269	36.09
	1-Palmitoyl lysophosphatidic acid	1.39517	0.5825	0.0773	409.2	438.6
	L-Malic acid	1.61052	0.6422	0.0776	133	736.7
	L-Leucine	4.68538	1.4571	0.0961	130.1	478.5
	Taurochenodeoxycholate	3.68048	0.4578	0.0963	498.3	279.6
	N2-Acetyl-L-ornithine	1.28345	2.2183	0.0989	173.1	679.5
	Adrenic acid	4.63707	1.1874	0.0992	331.3	65.96

UASPG, High-dose intervention group of polysaccharides from unprocessed *Angelica sinensis*.

number matching (<25 ppm) and the secondary spectrogram matching and searching the database of established standards of the laboratory. Hierarchical cluster analysis was used to verify the reliability of the differential metabolites in Table 5. The results showed the reasonability of the screened and identified differential metabolites under the positive- and negative-ion modes (Figure 7b). The KEGG pathway

TABLE 6 Enrichment analysis of KEGG pathway of different metabolites in the positive- and negative-ion mode between UASPG and the model group

Map name	Test	TestAll	Ref	RefAll	Test_per	Ref_per	*p*-Value	FDR	Rich factor
ABC transporters	14	49	138	3,116	28.57142857	4.428754814	1.03455×10^{-8}	5.17277×10^{-7}	0.101449275
Aminoacyl-tRNA biosynthesis	6	49	52	3,116	12.24489796	1.668806162	0.000129998	0.003249949	0.115384615
Valine, leucine and isoleucine biosynthesis	4	49	23	3,116	8.163265306	0.738125802	0.000383811	0.006396842	0.173913043
Purine metabolism	7	49	95	3,116	14.28571429	3.048780488	0.000590901	0.007386264	0.073684211
Valine, leucine and isoleucine degradation	4	49	42	3,116	8.163265306	1.3478819	0.00389518	0.038951802	0.095238095
Arginine biosynthesis	3	49	23	3,116	6.12244898	0.738125802	0.00518859	0.039782668	0.130434783
Biosynthesis of unsaturated fatty acids	5	49	74	3,116	10.20408163	2.374839538	0.005569574	0.039782668	0.067567568
Linoleic acid metabolism	3	49	28	3,116	6.12244898	0.898587933	0.009083497	0.056771855	0.107142857
Pyrimidine metabolism	4	49	65	3,116	8.163265306	2.086007702	0.018092179	0.100512106	0.061538462
Histidine metabolism	3	49	47	3,116	6.12244898	1.508344031	0.036522119	0.181333041	0.063829787
Caffeine metabolism	2	49	22	3,116	4.081632653	0.706033376	0.045818093	0.181333041	0.090909091
Taurine and hypotaurine metabolism	2	49	22	3,116	4.081632653	0.706033376	0.045818093	0.181333041	0.090909091
Neuroactive ligand–receptor interaction	3	49	52	3,116	6.12244898	1.668806162	0.047146591	0.181333041	0.057692308

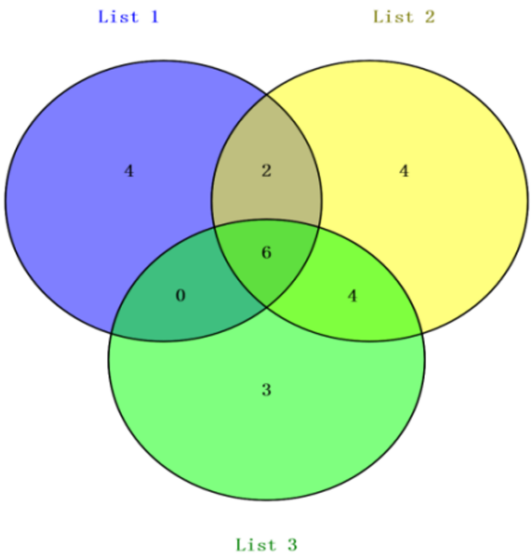

FIGURE 8 Combined analysis results of metabolic pathways. Note: list 1 represents the differential metabolic pathway between the control and model groups; list 2 represents the differential metabolic pathway between CASPG and the model group; and list 3 represents the differential metabolic pathway between UASPG and the model group

enrichment analysis of 75 selected differential metabolites was conducted using Fisher's exact test. The results revealed significant changes (Figure 7c, Rich factor > 0.05, *p*-value < 0.05) in 13 important metabolic pathways as follows: ABC transporters; aminoacyl-tRNA biosynthesis; valine, leucine and isoleucine biosynthesis; purine metabolism; valine, leucine and isoleucine degradation; arginine biosynthesis; biosynthesis of unsaturated fatty acids; linoleic acid metabolism; pyrimidine metabolism; histidine metabolism; caffeine metabolism; taurine and hypotaurine metabolism; and neuroactive ligand–receptor interaction. Moreover, these pathways were involved in amino acid metabolism disorder, unsaturated fatty acid biosynthesis, metabolic repair and so on. The specific parameters are shown in Table 6. Many previous studies have proved that *A. sinensis* polysaccharides has a good liver protection effect (Ma et al., 2020; Wang et al., 2017; Ye et al., 2001). The mass spectrum of the biomarkers in Tables 1, 3 and 5 are provided as Supplementary Materials.

3.1.6 | Conjoint analysis of the involved metabolic pathways

The Venn analysis method was used to complete the conjoint analysis based on the screened differential metabolic pathways and related differential metabolites to further analyze the differences in the intervention effect mechanism of CASP and UASP on the liver injury model of layer chicken induced by CS combined with LPS. The results in Figure 8 showed that the mutual differential metabolic pathways among all of the groups were ABC transporter, aminoacyl-tRNA biosynthesis, pyrimidine metabolism, histidine metabolism, valine, leucine and isoleucine biosynthesis, and linoleic acid metabolism. The respective metabolic pathways of all the groups are presented in Figure 9. The results of Figure 9 show that the occurrence mechanism of liver

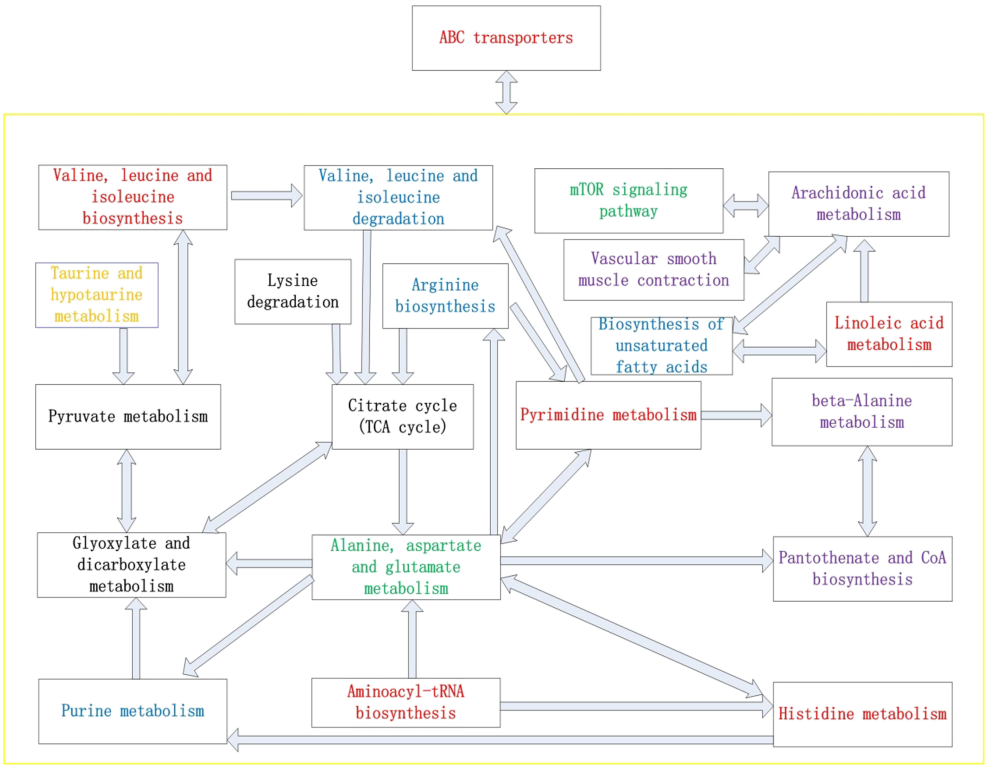

FIGURE 9 The conjoint analysis results of the hepatoprotective effect mechanism of CASPG and UASPG based on metabonomics. Note: the red mark represents the shared differential metabolic pathway among control group, model group, CASPG and UASPG. The green mark represents the shared differential metabolic pathway among control group, model group and CASPG. The black mark represents the screened differential metabolic pathway between the control and model groups. The purple mark represents the differential metabolic pathway between CASPG and the model group. The brown mark represents the differential metabolic pathway between UASPG and the model group. The blue mark represents the shared differential metabolic pathway among the model group, CASPG and UASPG

injury might lie in the affected ABC transporter pathway owing to LPS and CS. On the one hand, this phenomenon causes a series of amino acid metabolic disorders, leading to energy metabolism disorders; on the other hand, this phenomenon causes fatty acid metabolism disorders, resulting in the occurrence and development of the inflammatory reaction. The possible hepatoprotective effect mechanism of CASP may include the restoration of the disorder of amino and fatty acid metabolisms and the elimination of the inflammatory reaction through the intervention of the ABC transporter pathway. In contrast, the possible hepatoprotective effect mechanism of UASP may include the restoration of the amino acid, fatty acid and energy metabolism disorders through the intervention of the ABC transporter pathway.

ABC transporters can transport amino acids, nucleotides, sugars, vitamins and other macromolecular substances, such as polypeptides, proteins, cell metabolites and drugs (Glavinas et al., 2004). The differential metabolites of deoxyguanosine, deoxycytidine, deoxyinosine, hydroxyproline, L-histidine, inosine, L-valine, L-lysine, uridine, L-phenylalanine, L-glutamate, and L-leucine screened in this study were all in this pathway. The fold change values among different groups revealed that the contents of four metabolites (deoxyguanosine, deoxycytidine, deoxyinosine and hydroxyproline) increased after liver injury, while those of eight metabolites (L-histidine, inosine, L-valine, L-lysine, uridine, L-phenylalanine, L-glutamate and L-leucine) decreased after liver injury. Except for L-histidine, uridine, L-phenylalanine, and L-glutamate, the contents of eight other metabolites recovered after the intervention of CASP, and the contents of seven newly discovered differential metabolites (taurine, which increased significantly, adenosine, sucrose, cytidine, L-aspartate, L-arginine and L-glutamine), also decreased significantly.

Except for L-histidine, uridine, L-phenylalanine, L-glutamate and inosine, the contents of the seven other metabolites significantly recovered after the intervention withUASP. In addition, the contents of five newly discovered differential metabolites (taurine significantly increased, while sucrose, cytidine, L-aspartate and L-glutamine significantly decreased), and the increasing trend of taurine was lower than that of CASPG. The previous studies have confirmed that oxidative damage would destroy the activity of membrane transporters (Couteur et al., 1996; Prabhakar & Ibrahim, 2015). The analysis results of physiological and biochemical indices in the early stages also showed that the antioxidant effect on layer chickens after liver injury was significantly reduced ($p < 0.05$), and the changing trend in related metabolite contents among groups is shown in Tables 1, 3, and 5. The tables indicate that the liver injury induced by CS combined with LPS caused relatively severe oxidative stress damage to the liver cells of layer chickens.

Aminoacyl-tRNA biosynthesis, also known as the activation of amino acids, is an essential metabolic pathway in the process of

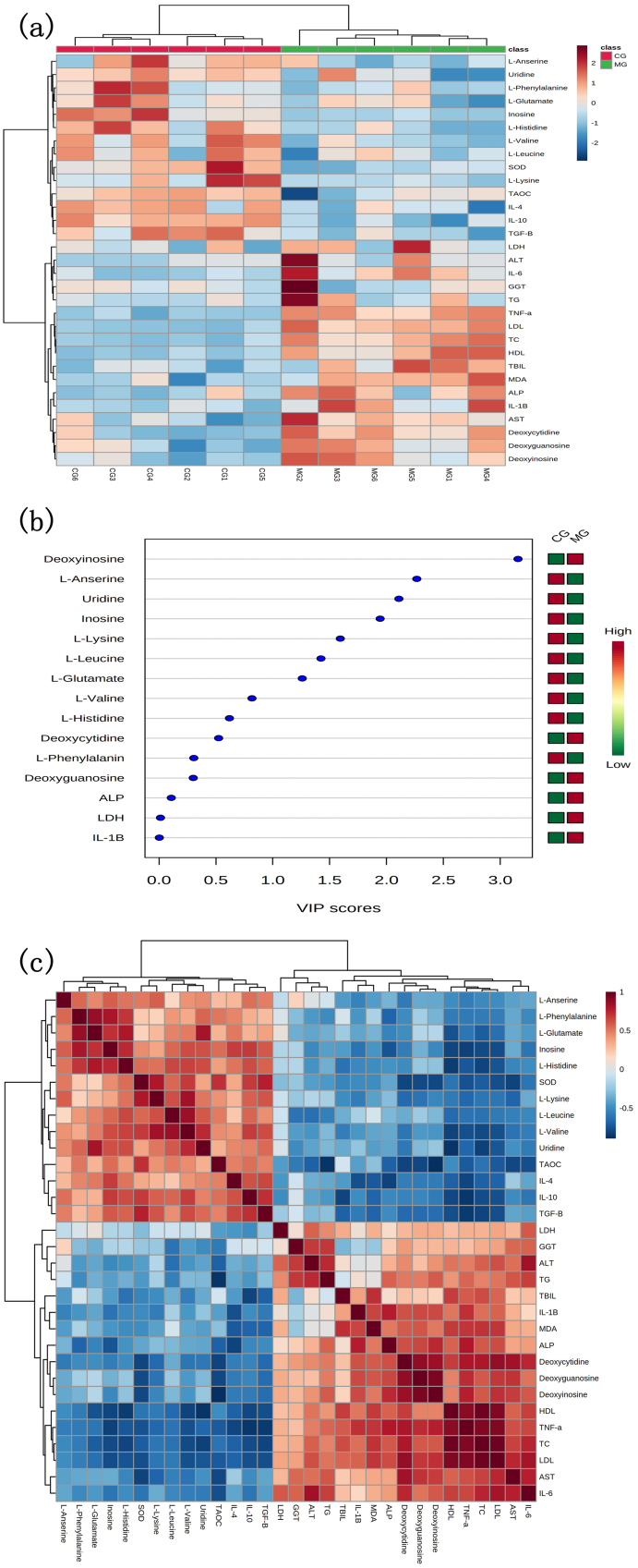

FIGURE 10 The heatmap analysis results (a), screened biomarkers (b) and correlation analysis results (c) of the control and model groups based on ABC transporters, aminoacyl-tRNA biosynthesis, valine, leucine and isoleucine biosynthesis and histidine metabolism. Note: CG, control group; MG, model group

protein synthesis (Guo et al., 2010). The results of this study showed that this pathway was closely related to the liver injury induced by CS combined with LPS, which was consistent with the previous study (Park et al., 2015). The differential metabolites (L-histidine, L-valine, L-lysine, L-phenylalanine, L-glutamate, and L-leucine) between the control and model groups were all in this pathway. The fold change value among the different groups revealed that six metabolites' contents (L-histidine, L-valine, L-lysine, L-phenylalanine, L-glutamate, and L-leucine) decreased after the appearance of liver injury. The contents of L-valine, L-lysine and L-leucine recovered after the intervention of CASP and those of three newly discovered differential metabolites (L-aspartate, L-arginine and L-glutamine) decreased. Meanwhile, the contents of L-valine, L-lysine, and L-leucine recovered after the intervention of UASP, and the trend was more evident than that of CASP. Moreover, L-glutamate was significantly decreased. In addition, a newly discovered differential metabolite (L-methionine) increased, and the changing trend in related metabolite contents among different groups is presented in Tables 1, 3 and 5.

Valine, leucine and isoleucine biosynthesis, one of the crucial amino acid synthesis pathways, is closely related to liver injury (Morgan et al., 1978). The results of this study showed that the metabolites of L-valine and L-leucine were all in the pathway. The fold change value of each group indicated that the metabolite contents of L-valine and L-leucine decreased after liver injury. The metabolite contents of L-valine and L-leucine recovered after the intervention of CASP and UASP. In addition, the contents of two newly discovered differential metabolites (ketoisocaproic acid and ketoleucine) increased, and the changing trend of related metabolite contents among different groups is presented in Tables 1, 3 and 5.

The mTOR signaling pathway, one of the critical inflammatory pathways, is also closely related to liver injury (Wei et al., 2020). This study showed that the mTOR signaling pathway was one of the pathways closely related to liver injury. L-Leucine is an essential metabolite of this pathway. The fold change value of each group revealed that the contents of L-Leucine decreased after liver injury. The metabolite contents of L-Leucine recovered after the intervention of CASP and UASP. In addition, the content of newly discovered differential metabolite (L-arginine) was decreased after the intervention of CASP and UASP. This reduction may be due to the consumption of L-arginine in large quantities to resist the liver injury induced by CS and LPS. The changing trend in related metabolite contents among different groups is presented in Tables 1, 3, and 5, consistent with the previous study (Li et al., 2012).

Alanine, aspartate and glutamate metabolism is a crucial metabolic pathway of amino acids (Wang et al., 2012). This study showed that L-glutamate and succinate were two important metabolic intermediates in the pathway. The fold change value among different groups revealed that the content of L-glutamate and succinate increased after liver injury, which was consistent with the previous study (Lieber et al., 1990). No significant change was observed after CASP and UASP interventions. The changing trend in related metabolite contents among different groups is presented in Tables 1, 3 and 5.

In addition, purine and pyrimidine metabolism was affected. Overall, the occurrence mechanism of the liver injury model of layer chickens induced by CS combined with LPS might lie in the effect of LPS and CS on the ABC transporter pathway. On the one hand, the phenomenon mentioned above causes a series of amino acid metabolic disorders, leading to energy metabolism disorder; on the other hand, this phenomenon also results in fatty acid metabolism disorder and promotes the occurrence and development of the inflammatory reaction. The possible hepatoprotective effect mechanism of CASP might include the restoration of the disorder of amino and fatty acid metabolisms and the elimination of the inflammatory reaction through the intervention of the ABC transporter pathway. Meanwhile, the possible hepatoprotective effect mechanism of UASP might restore the amino acid, fatty acid and energy metabolism disorders through the intervention of the ABC transporter pathway.

3.1.7 | Searching typical biomarkers of liver injury with thermography analysis, PLS-DA and correlation analysis

1. Study based on ABC transporters, aminoacyl-tRNA biosynthesis, valine, leucine and isoleucine biosynthesis, and histidine metabolism, as well as some important cell transmembrane- and amino acid-related metabolic pathways

Heat map analysis, PLS-DA and correlation analysis revealed that the physiological and biochemical indices detected in the early stage were combined with the screened recovery metabolites among ABC transporters and aminoacyl-tRNA biosynthesis, valine, leucine and isoleucine biosynthesis, and histidine metabolism associated with liver injury for conjoint analysis. The results are shown in Figure 10a–c. In Figure 10a, the liver injury model is proved successful based on the content changes in different metabolites and the physiological and biochemical indices in the cell transmembrane- and amino acid-related metabolic pathways screened in the previous stage. In Figure 10b, the specific biomarkers (VIP > 1.0) related to liver injury in this pathway include deoxyinosine, L-anserine, uridine, inosine, L-lysine, L-leucine and L-glutamate. In Figure 10c, among the seven typical biomarkers of liver injury, deoxyinosine was strongly positively correlated with the gold standard AST and ALT in the occurrence of liver injury. L-Anserine, uridine, inosine, L-lysine, L-leucine and L-glutamate were negatively correlated with AST and ALT, which could provide a new clinical indication for the occurrence of liver injury.

2. Study based on linoleic acid metabolism, mTOR signaling pathway, citrate cycle and other significant fatty acid metabolism-, energy metabolism- and inflammation-related metabolic pathways

Heat map analysis, PLS-DA and correlation analysis revealed that the physiological and biochemical indices detected in the early stages were combined with the selected metabolites related to liver injury in

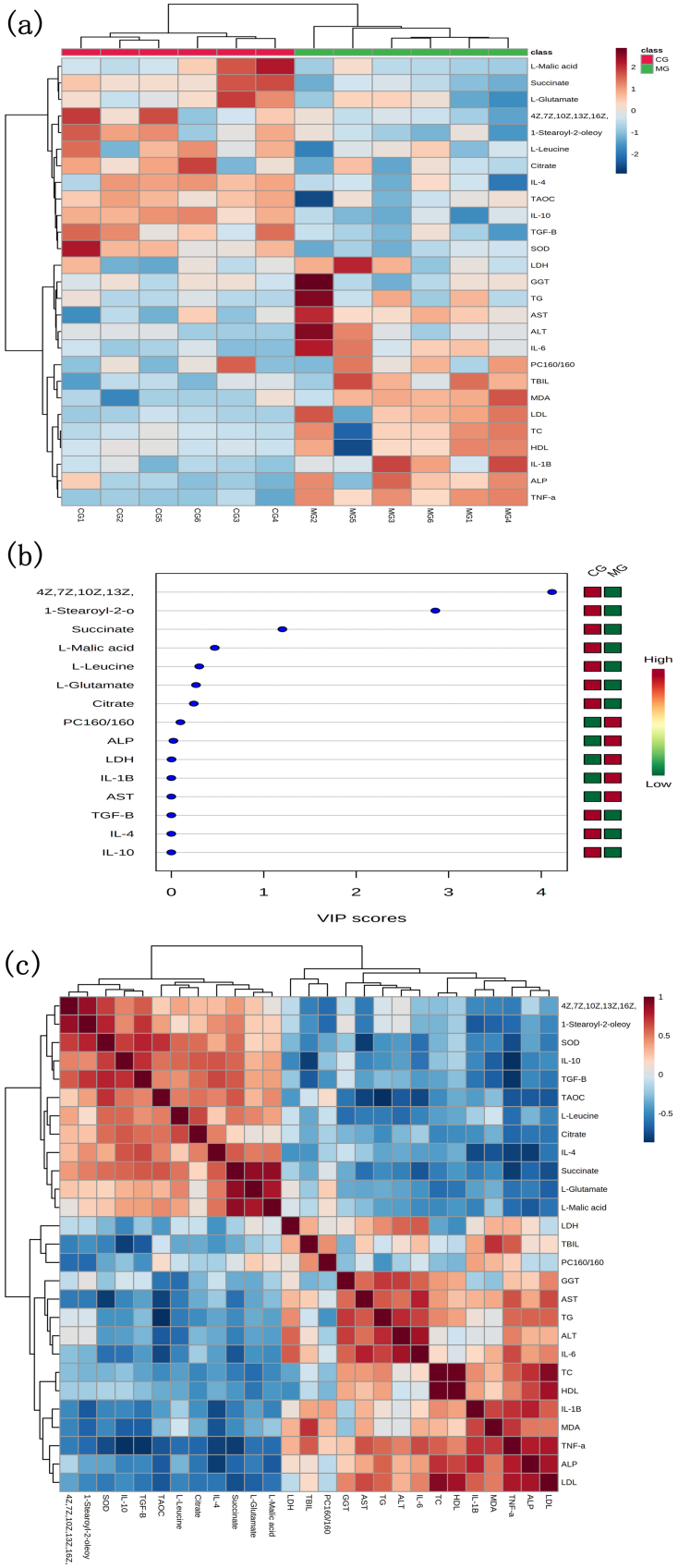

FIGURE 11 The heatmap analysis results (a), screened biomarkers (b) and correlation analysis results (c) of CG and MG based on linoleic acid metabolism, mTOR signaling pathway, citrate cycle, and other important fatty acid metabolism, energy metabolism and inflammation-related metabolic pathways

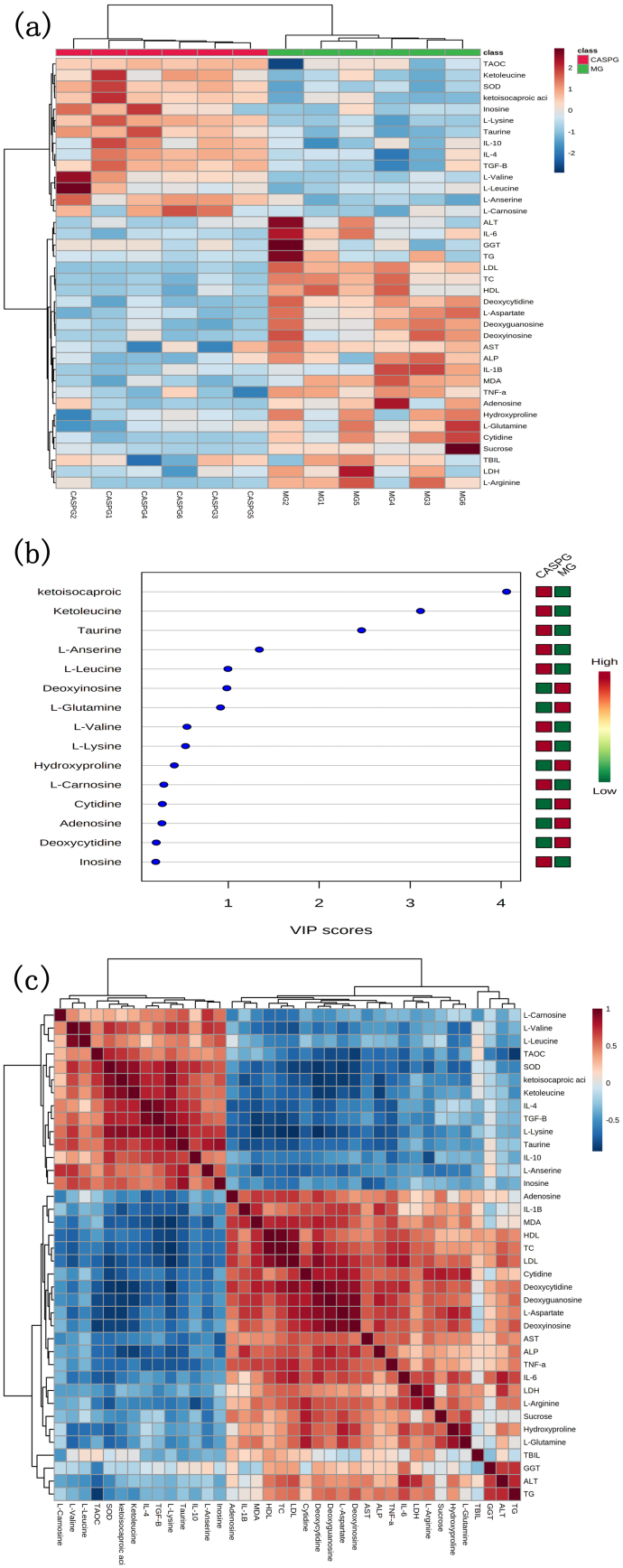

FIGURE 12 The heatmap analysis results (a), screened biomarkers (b) and correlation analysis results (c) of CASPG and MG based on ABC transporters, aminoacyl-tRNA biosynthesis, valine, leucine and isoleucine biosynthesis and histidine metabolism.

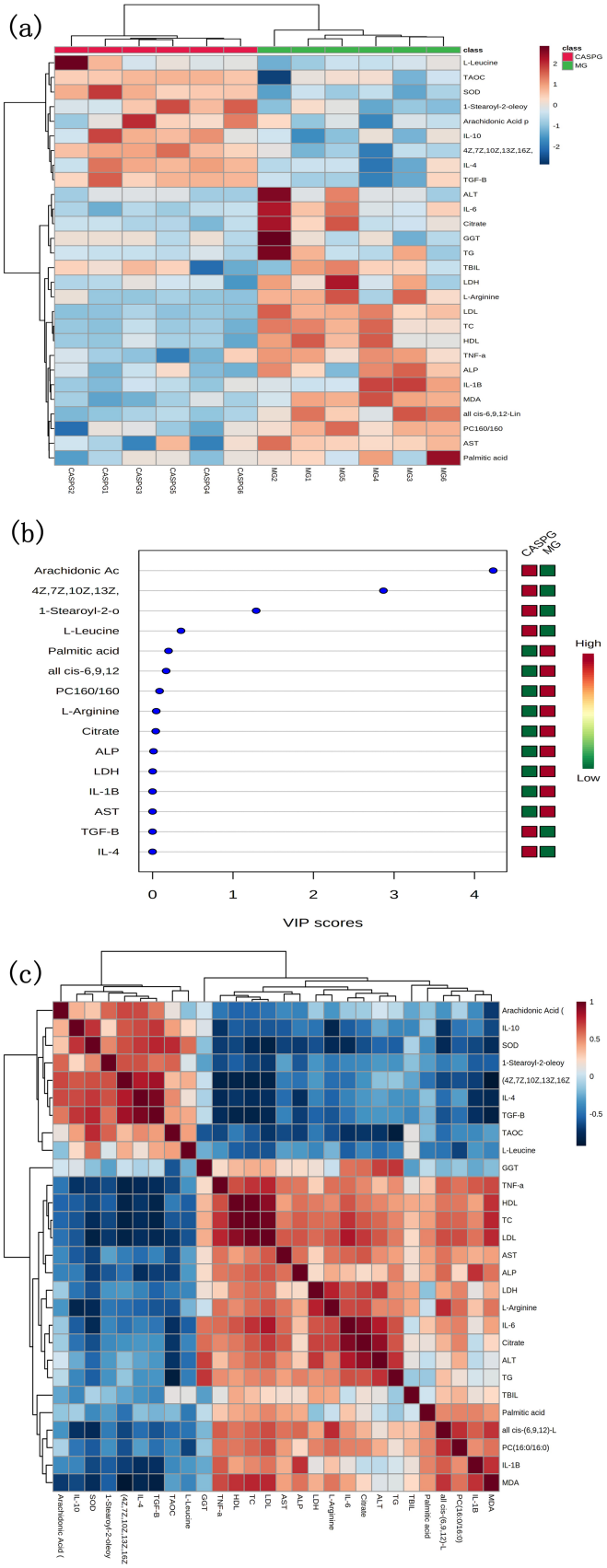

FIGURE 13 The heatmap analysis results (a), screened biomarkers (b) and correlation analysis results (c) of CASPG and MG based on linoleic acid metabolism, mTOR signaling pathway, biosynthesis of unsaturated fatty acids, and other important fatty acid metabolism, energy metabolism and inflammation-related metabolic pathways

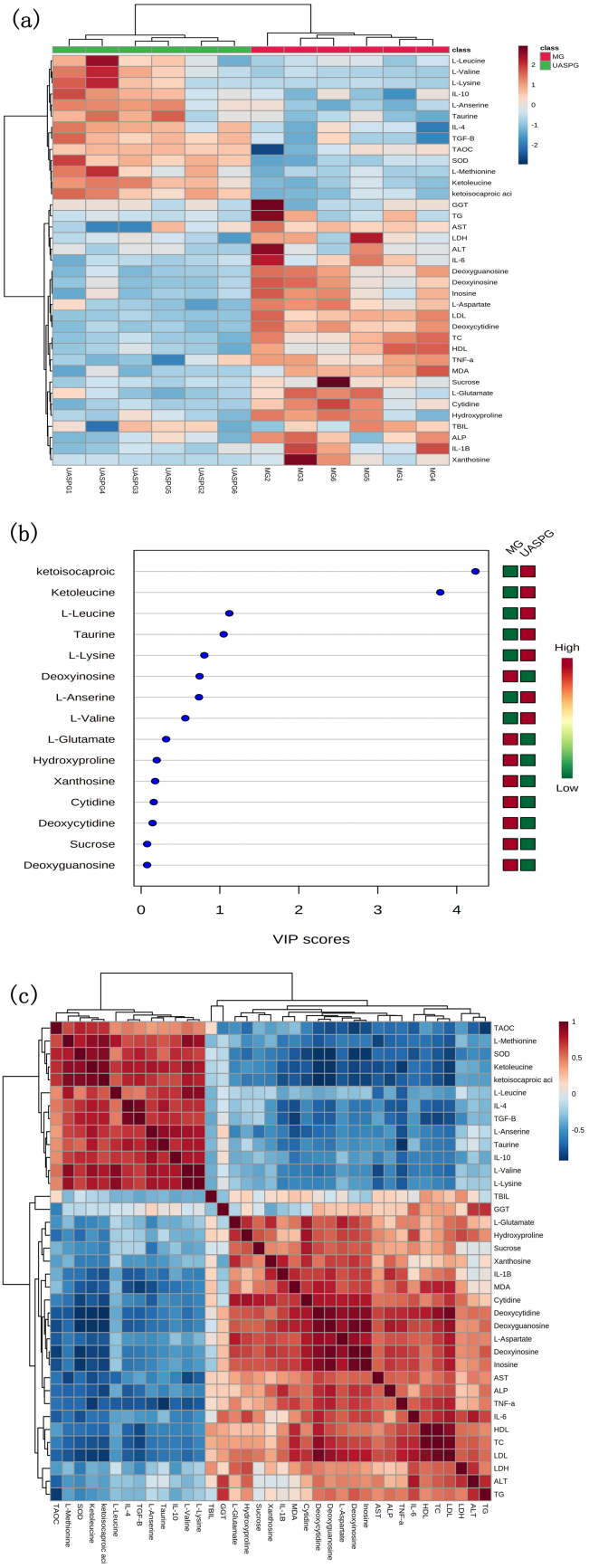

FIGURE 14 The heatmap analysis results (a), screened biomarkers (b) and correlation analysis results (c) of UASPG and MG based on ABC transporters, aminoacyl-tRNA biosynthesis, valine, leucine and isoleucine biosynthesis and histidine metabolism

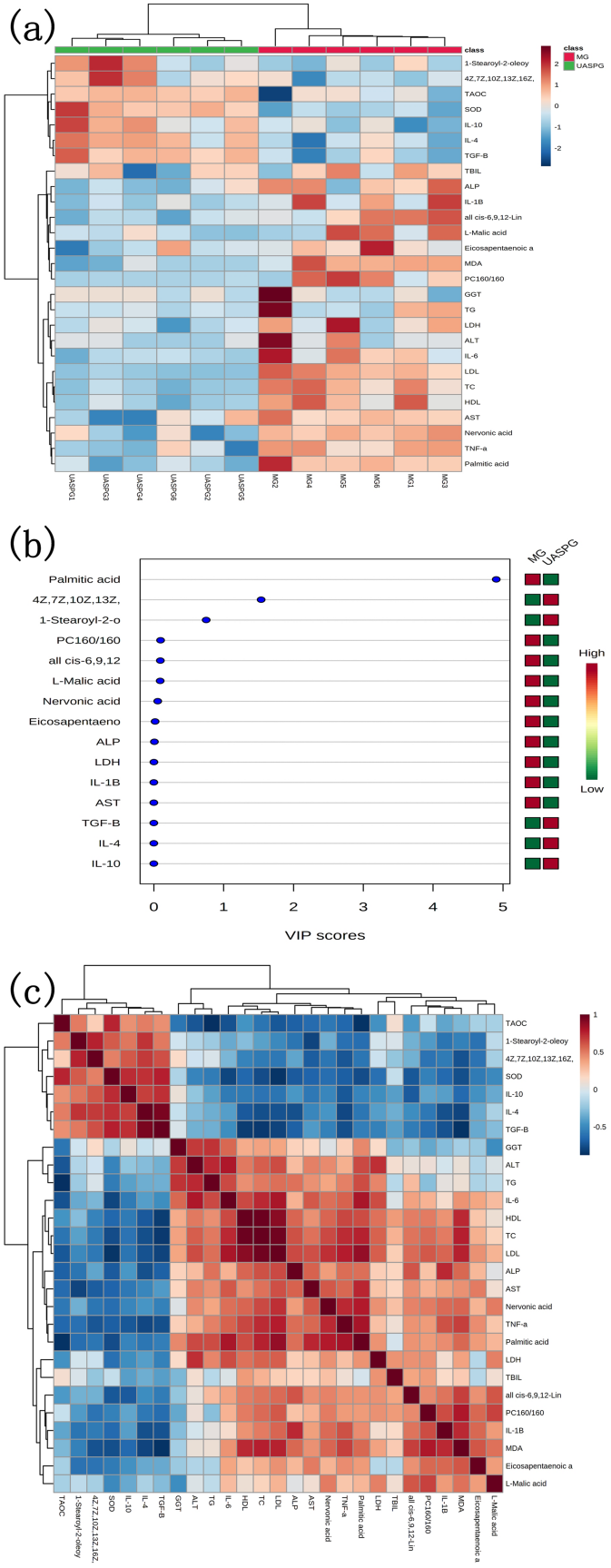

FIGURE 15 The heatmap analysis results (a), screened biomarkers (b) and correlation analysis results (c) of UASPG and MG based on linoleic acid metabolism, biosynthesis of unsaturated fatty acids, and other important fatty acid metabolism pathways

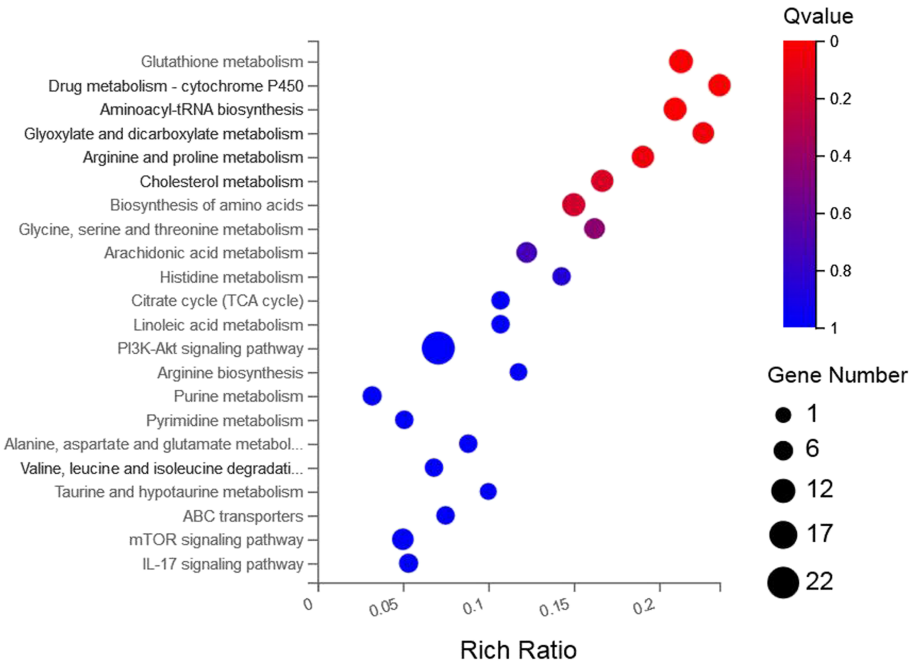

FIGURE 16 KEGG pathway enrichment analysis results based on transcriptome gene detection between all of the groups

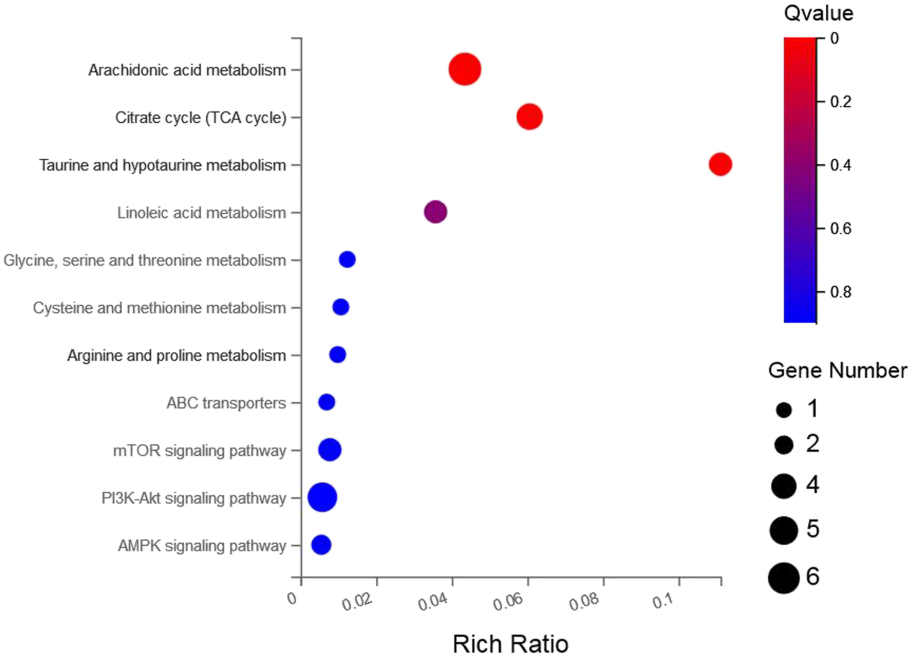

FIGURE 17 KEGG pathway enrichment analysis results based on transcriptome gene detection between CASPG and CG

the important fatty acid metabolism-, energy metabolism- and inflammation-related metabolic pathways for conjoint analysis. The results are shown in Figure 11a–c. In Figure 11a, the liver injury model was successfully verified based on the changes in metabolites and the physiological and biochemical indices of this pathway. In Figure 11b, the specific biomarkers (VIP > 1.0) closely related to liver injury in this pathway included (4Z,7Z,10Z,13Z,16Z,19Z)-4,7,10,13,16,19-docosahexenoic acid, 1-stearoyl-2-oleoyl-sn-glycerol-3-phosphate (SOPC) and succinate. In Figure 11c, the three typical biomarkers of liver injury are strongly negatively correlated with the occurrence of the gold standard of liver injury, AST, which could provide a new clinical indication for the occurrence of liver injury.

3.1.8 | Searching typical biological markers of liver protection of CASP with thermographic analysis, PLS-DA and correlation analysis

1. Study based on ABC transporters, aminoacyl tRNA biosynthesis, valine, leucine and isoleucine biosynthesis, and histidine

TABLE 7 KEGG pathway enrichment analysis results based on transcriptome gene detection between CASPG and the control group

KEGG pathway term Description	KEGG pathway	Term candidate gene number	Total candidate gene number	Term gene number	Total gene number	Rich ratio	*p*-Value	Q-Value
Arachidonic acid metabolism	Lipid metabolism	6	112	138	18,118	0.043478261	2.16×10^{-4}	0.04009438
Citrate cycle (TCA cycle)	Carbohydrate metabolism	4	112	66	18,118	0.060606061	7.43×10^{-4}	0.041953
Taurine and hypotaurine metabolism	Metabolism of other amino acids	3	112	27	18,118	0.111111111	6.04×10^{-4}	0.041953
Linoleic acid metabolism	Lipid metabolism	3	112	84	18,118	0.035714286	0.0152508	0.43083454
Glycine, serine and threonine metabolism	Amino acid metabolism	1	112	81	18,118	0.012345679	0.3955203	0.89956547
Cysteine and methionine metabolism	Amino acid metabolism	1	112	94	18,118	0.010638298	0.4425536	0.89956547
Arginine and proline metabolism	Amino acid metabolism	1	112	102	18,118	0.009803922	0.469675	0.89956547
ABC transporters	Membrane transport	1	112	145	18,118	0.006896552	0.5945394	0.89956547
mTOR signaling pathway	Signal transduction	3	112	388	18,118	0.007731959	0.431332	0.89956547
PI3K-Akt signaling pathway	Signal transduction	5	112	871	18,118	0.005740528	0.6303383	0.89956547
AMPK signaling pathway	Signal transduction	2	112	365	18,118	0.005479452	0.6628812	0.89956547

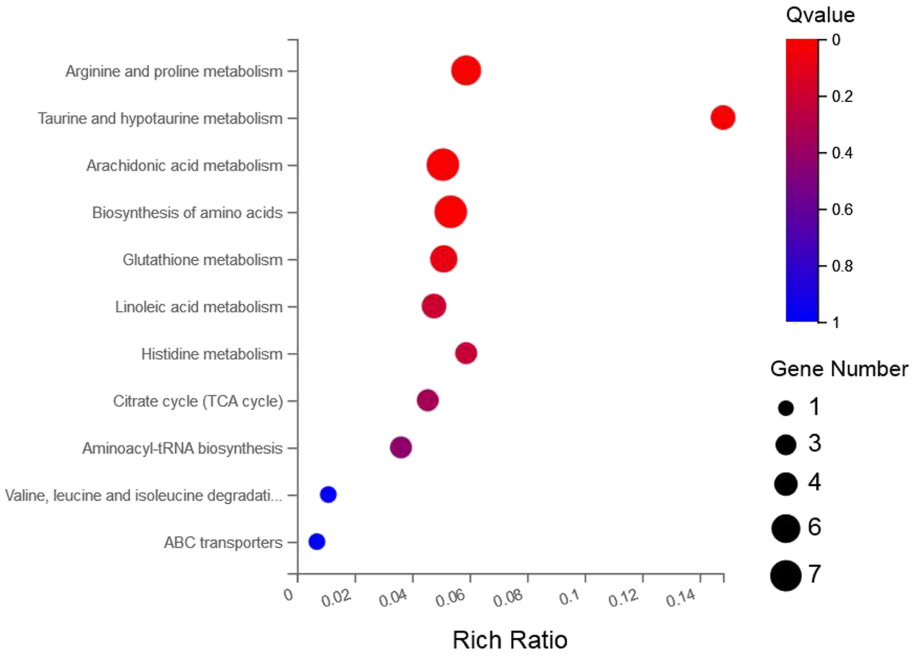

FIGURE 18 KEGG pathway enrichment analysis results based on transcriptome gene detection between UASPG and CG

metabolism, as well as some important cell transmembrane- and amino acid-related metabolic pathways

Heat map analysis, PLS-DA and correlation analysis revealed that the physiological and biochemical indices detected in the early stages were combined with the screened recovery metabolites among ABC transporters and aminoacyl-tRNA biosynthesis, valine, leucine and isoleucine biosynthesis, and histidine metabolism associated with liver injury for conjoint analysis. The results are shown in Figure 12a–c. In Figure 12a, the liver injury model is proved successful based on the

TABLE 8 KEGG pathway enrichment analysis results based on transcriptome gene detection between UASPG and the control group

KEGG pathway term Description	KEGG pathway	Term candidate gene number	Total candidate gene number	Term gene number	Total gene number	Rich ratio	*p*-Value	Q-Value
Arginine and proline metabolism	Amino acid metabolism	6	167	102	18,118	0.0588235	3.64×10^{-4}	0.02145731
Taurine and hypotaurine metabolism	Metabolism of other amino acids	4	167	27	18,118	0.1481481	1.04×10^{-4}	0.02145731
Arachidonic acid metabolism	Lipid metabolism	7	167	138	18,118	0.0507246	2.94×10^{-4}	0.02145731
Biosynthesis of amino acids	Global and overview maps	7	167	131	18,118	0.0534351	2.13×10^{-4}	0.02145731
Glutathione metabolism	Metabolism of other amino acids	5	167	98	18,118	0.0510204	0.002135	0.10075062
Linoleic acid metabolism	Lipid metabolism	4	167	84	18,118	0.047619	0.007585	0.21807032
Histidine metabolism	Amino acid metabolism	3	167	51	18,118	0.0588235	0.011588	0.24441969
Citrate cycle (TCA cycle)	Carbohydrate metabolism	3	167	66	18,118	0.0454545	0.023047	0.36259874
Aminoacyl-tRNA biosynthesis	Translation	3	167	83	18,118	0.0361446	0.041364	0.44371926
Valine, leucine and isoleucine degradation	Amino acid metabolism	1	167	92	18,118	0.0108696	0.574328	0.9974545
ABC transporters	Membrane transport	1	167	145	18,118	0.0068966	0.740268	0.9974545

content changes in different metabolites and the physiological and biochemical indices. In Figure 12b, the typical biomarkers (VIP > 1.0) closely related to the hepatoprotective effect in this metabolic pathway include ketoisopronic acid, ketoleucine, taurine, L-anserine, L-leucine and deoxyinosine. In Figure 12c, among the most important biomarkers, ketoisocaproic acid, ketoleucine, taurine, L-anserine and L-leucine are negatively correlated with AST and ALT, which could provide new clinical indications for the mechanism of CASP in the treatment of liver injury induced by CS combined with LPS.

2. Study based on linoleic acid metabolism, mTOR signaling pathway, biosynthesis of unsaturated fatty acids, and other essential fatty acid metabolism-, energy metabolism- and inflammation-related metabolic pathways

Heat map analysis, PLS-DA and correlation analysis revealed that the physiological and biochemical indices detected in the early stages were combined with the screened recovery metabolites among the related metabolic pathways of fatty acid metabolism-, energy metabolism- and inflammation-related metabolic pathways for conjoint analysis. The results are shown in Figure 13a–c. It can be seen that the significant recovery of liver injury is verified based on the changes in metabolites and the physiological and biochemical indices of this pathway in Figure 13a. The typical biomarkers (VIP > 1.0) closely related to the hepatoprotective effect in this pathway were arachidonic acid (peroxidate free) and SOPC in Figure 13b. According to Figure 13c, the above three typical biomarkers related to the hepatoprotective effect had strong negative correlations with AST and malonaldehyde (MDA). They had strong positive correlations with superoxide dismutase (SOD). This could provide the basis and new clinical indications for the mechanism of CASP in the treatment of liver injury induced by CS combined with LPS.

3.1.9 | Searching typical biomarkers for liver protection of USAP with thermographic analysis, PLS-DA and correlation analysis

1. Study based on ABC transporters, aminoacyl-tRNA biosynthesis, valine, leucine and isoleucine biosynthesis and histidine metabolism, as well as some important cell transmembrane- and amino acid-related metabolic pathways

TABLE 9 Differential expression of genes related to arachidonic acid metabolic pathway between all of the groups

Gene symbol	Type	log2 (MG/CG)	Q-Value (MG/CG)	log2 (CASPG/MG)	Q-Value (CASPG/MG)	log2 (UASPG/MG)	Q-Value (UASPG/MG)	log2 (CASPG/CG)	Q-Value (CASPG/CG)	log2 (UASPG/CG)	Q-Value (UASPG/CG)	log2 (CASPG/UASPG)	Q-Value (CASPG/UASPG)
HPGDS	mRNA	0.203	0.663	−0.18	0.517	−0.371	0.042	0.022	0.986	−0.169	0.787	0.191	0.71
GGT2	mRNA	−5.632	0.005	0.727	0.757	−0.264	0.996	−4.906	0.068	−5.901	0.003	0.993	0.532
CBR3	mRNA	−0.205	0.964	−0.45	0.027	−0.204	0.545	−0.652	0.473	−0.41	0.701	−0.242	0.335
CYP2J23	mRNA	0.419	0.172	−0.51	0.025	0.074	0.996	−0.09	0.957	0.491	0.019	−0.582	0.0002
LTC4SL	mRNA	0.568	0.186	−0.22	0.875	0.172	0.925	0.348	0.676	0.74	0.01	−0.39	0.456
PLA2G4EL2	mRNA	−7.124	0.316	−0.45	0.985	1.011	0.996	−22.024	0	−5.475	0.403	−1.454	0.989

MG, Model group; CG, control group.

TABLE 10 Differential expression of genes related to the mTOR signaling pathway based on transcripts between all of the groups

Gene symbol	Type	log2 (MG/CG)	Q-Value (MG/CG)	log2 (CASPG/MG)	Q-Value (CASPG/MG)	log2 (UASPG/MG)	Q-Value (UASPG/MG)	log2 (CASPG/CG)	Q-Value (CASPG/CG)	log2 (UASPG/CG)	Q-Value (UASPG/CG)	log2 (CASPG/UASPG)	Q-Value (CASPG/UASPG)
SESN2	mRNA	−0.0239	0.9837	0.0397	0.9851	−0.7670	0.0006	0.0168	0.9899	−0.7912	0.0000	0.8081	0.0005
LOC107051846	mRNA	0.2987	0.2286	0.2062	0.6461	−0.2787	0.2203	0.5051	0.0478	0.0194	0.9900	0.4858	0.0127
FZD4	mRNA	0.3756	0.3426	−0.6269	0.0191	−0.2598	0.6848	−0.2503	0.6292	0.1151	0.9039	−0.3655	0.2803
CLIP1	mRNA	−0.4817	0.0307	0.2923	0.1793	0.1355	0.7861	−0.1883	0.7490	−0.3468	0.2236	0.1583	0.7560
ULK1	mRNA	0.2679	0.5917	−0.5576	0.0143	0.0664	0.9955	−0.2888	0.5218	0.3339	0.5538	−0.6228	0.0391
GATSL2	mRNA	−0.3330	0.8640	0.4341	0.3767	0.6686	0.0386	0.1016	0.9860	0.3350	0.7795	−0.2317	0.5978
ULK2	mRNA	1.1864	0.0015	−0.8508	0.4483	−1.4464	0.0000	0.3372	0.8608	−0.2606	0.7478	0.5977	0.6930

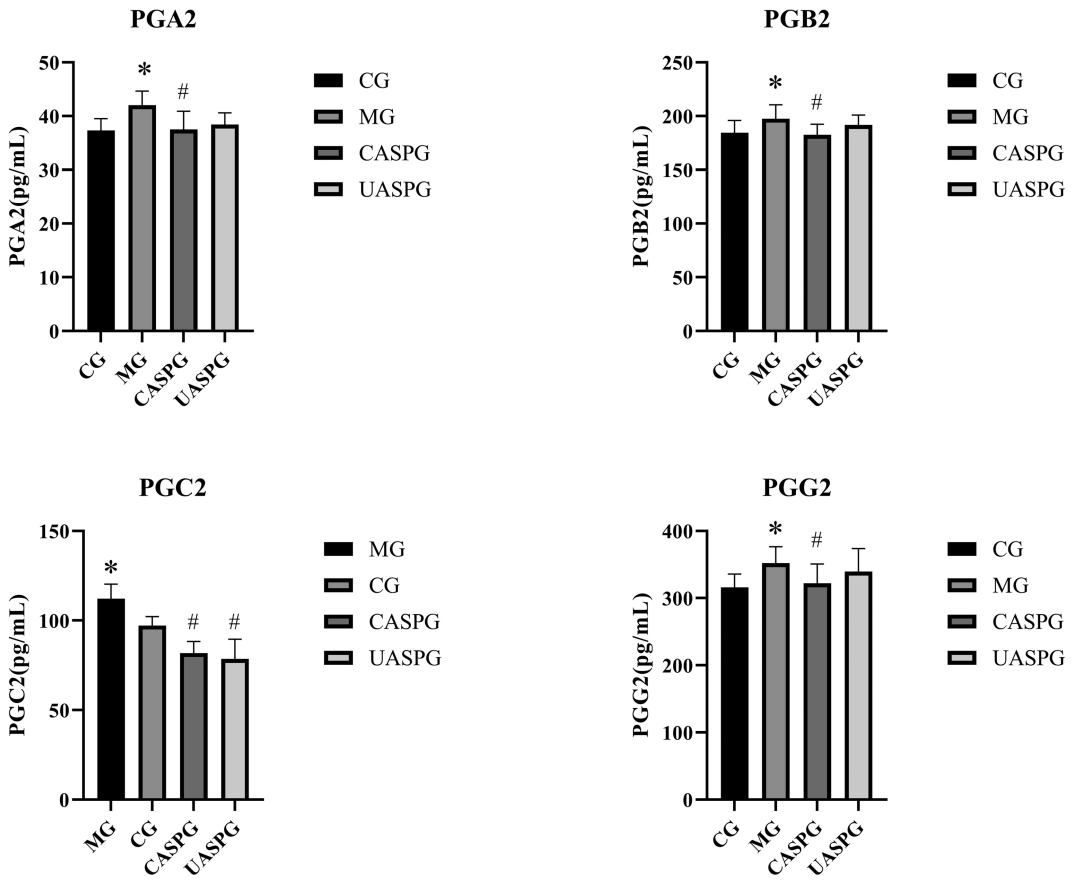

FIGURE 19 ELISA detection and analysis results of PGA2, PGB2, PGC2 and PGG2 between all of the groups

Heat map analysis, PLS-DA and correlation analysis revealed that the physiological and biochemical indices detected in the early stage were combined with the screened recovery metabolites among ABC transporters and aminoacyl tRNA biosynthesis, valine, leucine and isoleucine biosynthesis, and histidine metabolism associated with liver injury for conjoint analysis. The results are shown in Figure 14a–c. In Figure 14a, the repair of liver injury is successful based on the change level of metabolites in these pathways, and physiological and biochemical indices. In Figure 14b, it can be seen that the typical biomarkers (VIP > 1.0) closely related to the repair of liver injury in this pathway include ketoisocaloric acid, ketoleucine, taurine and L-leucine. In Figure 14c, the four kinds of typical biomarkers have a strong negative correlation with AST and ALT. These results could provide evidence and new clinical indications for the mechanism of UASP in the treatment of liver injury induced by CS combined with LPS.

2. Study based on linoleic acid metabolism, biosynthesis of unsaturated fatty acids, and other important fatty acid metabolism-, energy metabolism- and inflammation-related metabolic pathways

Based on heat map analysis, PLS-DA and correlation analysis, the physiological and biochemical indices detected in the early stage were combined with the screened recovery metabolites among the related metabolic pathways of fatty acid metabolism-, energy metabolism- and inflammation-related metabolic pathways metabolites which were associated with liver damage repair for conjoint analysis. The results are shown in Figure 15a–c. In Figure 15a, it can be seen the liver damage repair was successful based on the pathway of metabolites and physiological and biochemical indices content change levels; in Figure 15b, the typical biomarkers (VIP > 1.0) closely related to the hepatoprotective effect in this pathway are palmitic acid and (4Z,7Z,10Z,13Z,16Z,19Z)-4,7,10,13,16,19-docosahexenoic acid. In Figure 15c, palmitic acid strongly correlates with AST and ALT. (4Z,7Z,10Z,13Z,16Z,19Z)-4,7,10,13,16,19-Docosahexaenoic acid has a strong negative correlation with AST and ALT. These results could provide evidence and new clinical indications for the mechanism of UASP in the treatment of liver injury induced by CS combined with LPS.

3.2 | The biological verification results

3.2.1 | Liver transcriptomics detection and analysis results

Through liver tissues transcriptomic detection and KEGG pathway enrichment analysis of each group, we found that the pathway

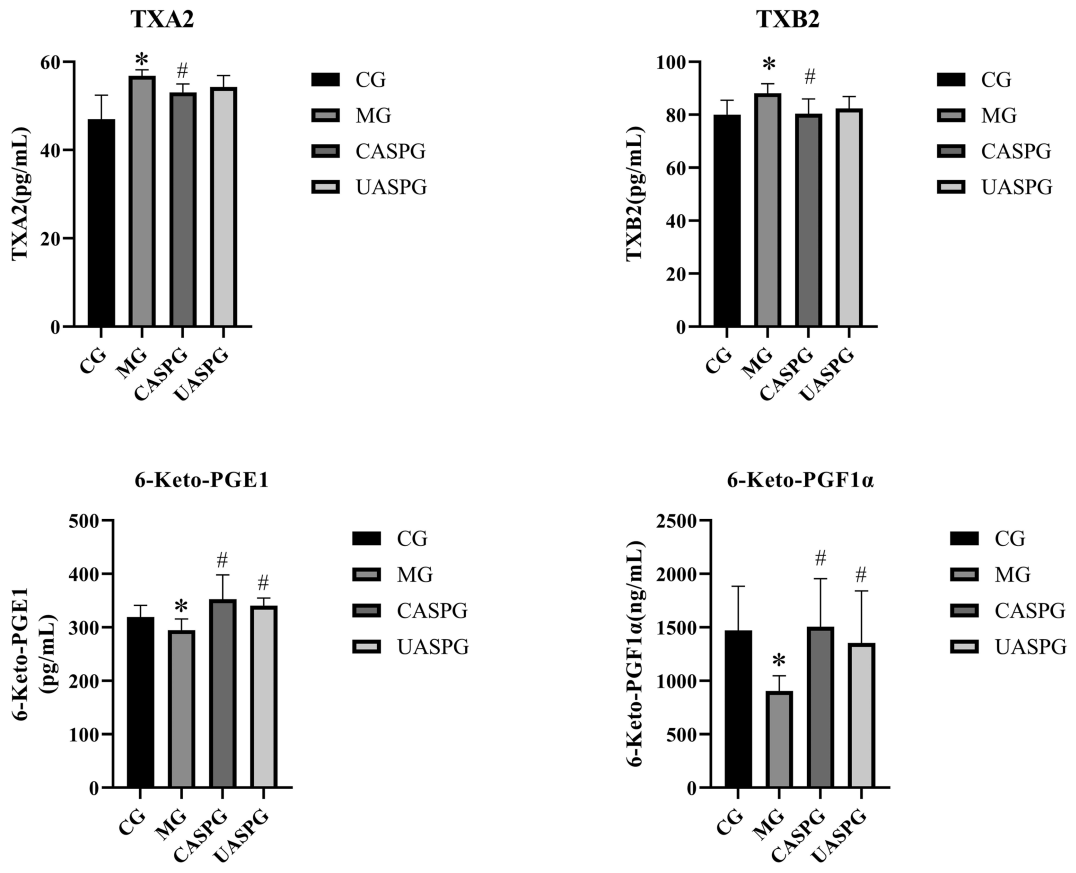

FIGURE 20 ELISA detection and analysis results of TXA2, TXB2, 6-keto-PGE1 and 6-keto-PGF1αbetween all of the groups

enrichment results (Figure 16) were consistent with the previous metabolomic pathway analysis results (Figure 9, Tables 2, 4 and 6), mainly involving amino acid metabolism, lipid metabolism and important signal pathways involved in cell proliferation and protein synthesis. In addition, it was found that CASP mainly could improve the liver protection ability of chickens through the pathways in Figure 17 and Table 7, and UASP mainly could improve the liver protection ability of chickens through the pathways in Figure 18 and Table 8. Among them, we found that arachidonic acid metabolism and the mTOR signal pathway were indeed affected, following the pathway analysis results in the metabonomic study. The gene expression analysis results related to the arachidonic acid metabolism pathway are provided in Table 9. The gene expression analysis results related to the mTOR signal pathway are provided in Table 10.

In Table 9, the results showed that, after CASP intervention, the content expression of PLA2G4EL2 in the liver of the control group decreased significantly ($p < 0.05$), indicating that CASP might significantly inhibit the biosynthesis of the arachidonic acid metabolic upstream pathway. After CASP intervention on MG, the expression of CYP2J23 and CBR3 in chicken liver decreased significantly ($p < 0.05$), indicating that CASP might significantly inhibit the biological metabolism of the arachidonic acid metabolic downstream pathway, which is consistent with the analysis results of metabolomics. Compared with the normal group, the expression of CYP2J23 and LTC4SL in chicken liver increased significantly ($p < 0.05$), and the expression of GGT2 decreased significantly ($p < 0.05$), indicating that UASP might promote the degradation of arachidonic acid by affecting the metabolism of cytochrome P450 to a certain extent, and might promote the metabolism of leukotriene C4 downstream of the arachidonic acid metabolic pathway.

In Table 10, the results show that, compared with the control group, the expression content of CLIP1 in chicken liver tissue decreased significantly after liver injury ($p < 0.05$), indicating that the metabolism of microtubule organization downstream of the mTOR signaling pathway might be inhibited after liver injury, while the expression content of ULK2 in liver tissue increased significantly ($p < 0.05$), indicating that the autophagy of hepatocytes downstream of the mTOR signaling pathway might be strengthened after liver injury. Compared with the model group, after CASP intervention, the expression of FZD4 and ULK1 in chicken liver decreased significantly ($p < 0.05$), indicating that CASP might significantly inhibit the synthesis of the mTOR signaling pathway by the Wnt pathway upstream of the mTOR signaling pathway and the autophagy of hepatocytes downstream of the mTOR signaling pathway. Compared with the model group, the expression of SESN2 in chicken liver decreased significantly after UASP intervention ($p < 0.05$), indicating that UASP might significantly inhibit the synthesis of mTOR through leucine upstream of the mTOR signaling pathway. In addition, compared with the control group, the expression of LOC107051846 in chicken liver increased significantly after CASP prevention treatment ($p < 0.05$),

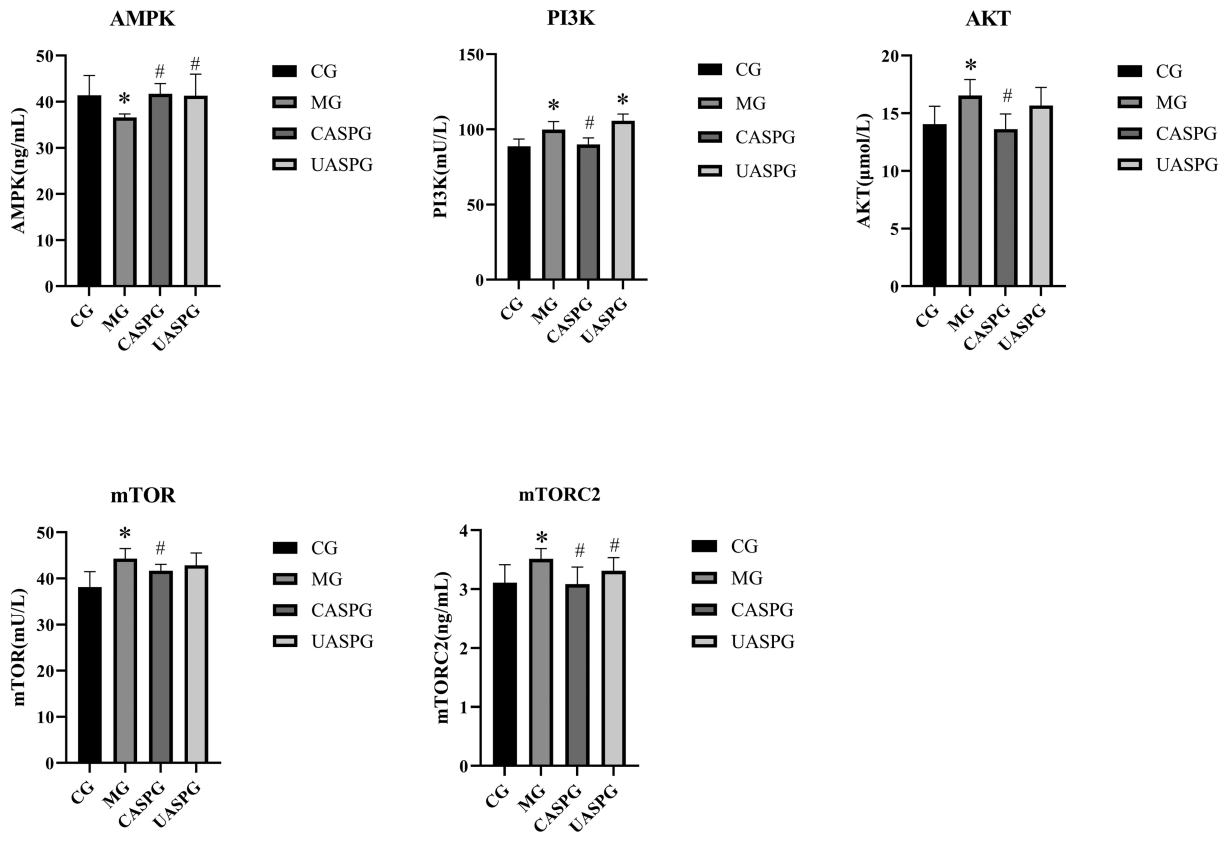

FIGURE 21 ELISA detection and analysis results of AMPK, AKT, MTOR, MTORC2 and PI3K between all of the groups

indicating that CASP might intervene in the synthesis of mTOR by intervening in the PI3K/Akt pathway to a certain extent.

3.2.2 | ELISA detection and analysis results

It is reported that TXA2, TXB2 and 6-keto-PGF1α in the arachidonic acid metabolic pathway and AMPK, AKT, mTOR, MTORC2, PI3K in the mTOR signaling pathway have a close relationship with liver injury (Ćavar et al., 2017; Cao et al., 2017; Fan et al., 2018; Nagai et al., 1989; Peng et al., 2008; Yang, Zhao, et al., 2019; Zhou et al., 2020; Zhu et al., 2015). Therefore further pathway verification was carried out. The ELISA method was used to analyze the changing trends of TXA2, TXB2, 6-keto-PGF1α and 6-keto-PGE1 and the related PGA2, PGB2, PGC2 and PGG2 in the arachidonic acid metabolic pathway and AMPK, AKT, mTOR, MTORC2 and PI3K in the mTOR signaling pathway in each group. The results are shown in Figures 19–21. In Figures 19 and 20, compared with the control group, the contents of PGA2, PGB2, PGC2, PGG2, TXA2 and TXB2 in the model group were increased significantly ($p < 0.05$) and the contents of 6-keto-PGE1 and 6-keto-PGF1α decreased significantly ($p < 0.05$). Compared with the model group, the contents of PGA2, PGB2, PGC2, PGG2, TXA2 and TXB2 in serum from the CASPG decreased significantly ($p < 0.05$) and the contents of 6-keto-PGE1 and 6-keto-PGF1α increased significantly ($p < 0.05$). Compared with the model group, the content of PGC2 in the serum from the UASPG decreased significantly ($p < 0.05$) and the contents of 6-keto-PGE1 and 6-keto-PGF1α increased significantly ($p < 0.05$). The results are consistent with previous results. In Figure 21, compared with the control group, the contents of AKT, mTOR, MTORC2 and PI3K in the model group were significantly increased ($p < 0.05$) and the contents of AMPK decreased significantly ($p < 0.05$). Compared with the model group, the contents of AKT, mTOR, MTORC2, and PI3K in the serum from the CASPG decreased significantly ($p < 0.05$) and the contents of AMPK increased significantly ($p < 0.05$). Compared with the model group, the content of MTORC2 in the serum from the UASPG decreased significantly ($p < 0.05$) and the contents of AMPK increased significantly ($p < 0.05$).

To a certain extent, the above results confirmed the biological verification for the two metabolic pathways (arachidonic acid metabolism and mTOR signaling pathway) obtained from the enrichment analysis comprehensive results of metabonomics and transcriptomics.

4 | CONCLUSION

Combined with the results of clinical indications observation, physiological and biochemical indices, antioxidant indices, immune-inflammatory factors and the UPLC–Q/TOF–MS/MS metabonomics, the results of the conjoint analysis showed that CS combined with LPS could affect the transmembrane transport, amino acid metabolism, fatty acid metabolism,

tricarboxylic acid cycle, mTOR and other critical metabolic pathways in layer chickens and cause liver injury. The specific biomarkers closely related to the occurrence of liver injury included deoxyinosine, L-anserine, uridine, inosine, L-lysine, L-leucine, L-glutamate, arachidonic acid (peroxide free), (4Z,7Z,10Z,13Z,16Z,19Z)-4,7,10,13,1,6,19-docosahexaenoic acid and SOPC. The following conditions were observed after the occurrence of the above metabolic disorder: the content of MDA in liver tissue increased, the content of SOD decreased, liver oxidative stress injury occurred, the level of pro-inflammatory factors increased, the level of anti-inflammatory factors decreased, and an inflammatory reaction occurred, leading to liver cell swelling, degeneration, necrosis and partial liver fibrosis. Thus, these conditions significantly increased the serum AST, ALT, total bilirubin, low-density lipoprotein cholesterol and other indicators.

With the comprehensive analysis of the above results based on the metabonomics, transcriptomics and ELISA, we found that the chicken liver injury and the hepatoprotective effect mechanism of CASP and UASP were related to the arachidonic acid metabolism and mTOR signaling pathway. Overall, the prevention and treatment effect of CASP was better than that of UASP. The hepatoprotective effect mechanism of CASP was mainly involved in restoring arachidonic acid metabolism, the mTOR signaling pathway and other critical disordered metabolic pathways, including transmembrane transport, amino acid metabolism and linoleic acid metabolism. The specific biomarkers closely related to the hepatoprotective effect of CASP were ketoisocaloric acid, ketoleucine, taurine, L-anserine, L-leucine, deoxyinosine, arachidonic acid (peroxide free), (4Z,7Z,10Z,13Z,16Z,19Z)-4,7,10,13,16,19-docosahexaenoic acid and SOPC. The prevention and treatment of CASP resulted in the following conditions: the related metabolic pathway callback, the content of MDA in liver tissue significantly decreased, the content of SOD significantly increased, the degree of oxidative stress injury weakened, the level of anti-inflammatory factors increased, the level of pro-inflammatory factors decreased, the degree of vacuolar degeneration and necrosis of hepatocytes reduced, the damaged hepatocytes were repaired, and the contents of AST, ALT, total bilirubin and low-density lipoprotein in the serum reduced. The hepatoprotective effect mechanism of UASP was mainly related to the arachidonic acid metabolism, transmembrane transport, amino acid metabolism, linoleic acid metabolism and other important metabolic pathways. The specific biomarkers closely related to the hepatoprotective effect of UASP were ketoisocarbonic acid, ketoleucine, taurine, L-leucine, palmitic acid, and (4Z,7Z,10Z,13Z,16Z,19Z)-4,7,10,13,16,19-docosahexaenoic acid.

CONFLICT OF INTEREST

All the authors confirm that no conflicts of interest exist.

FUNDING

The study was sponsored by a University-level Fuxi talent project (Gaufx-02Y05), National Natural Science Foundation of China (31602102), and by the Lanzhou talent innovation and entrepreneurship project (2021-RC-57). The authors state that there is no conflict of interest. All procedures in this research involving animals conform to the ethical standards of national forensic services.

AUTHORS' CONTRIBUTIONS

Fanlin Wu, Yonghao Hu and Peng Ji conceived the project, designed the experiments and wrote this paper. Fanlin Wu, Peng Ji, Chenchen Li and Jian He performed the experiments. Fanlin Wu and Peng Ji performed computational analysis. Fanlin Wu wrote the manuscript. Fanlin Wu, Yonghao Hu and Peng Ji revised the manuscript.

ORCID

Peng Ji https://orcid.org/0000-0002-6041-0189

REFERENCES

Bogdanovska, L., Poceva Panovska, A., Popovska, M., Dimitrovska, A., & Petkovska, R. (2017). Chemometric evaluation of the efficacy of locally administered chlorhexidine in patients with periodontal disease. *Journal Saudi Pharmaceutical*, *25*(7), 1022–1031. https://doi.org/10.1016/j.jsps.2017.03.006

Cao, M. N., Wang, H. X., Guo, L. M., Yang, S. M., Liu, C., Khor, T. O., Yu, S. W., & Kong, A. N. (2017). Dibenzoylmethane protects against ccl4-induced acute liver injury by activating nrf2 via jnk, ampk, and calcium signaling. *The AAPS Journal*, *19*, 1703–1714. https://doi.org/10.1208/s12248-017-0133-1

Ćavar, I., Kelava, T., Pravdić, D., & Čulo, F. (2017). Anti-thromboxane b2 antibodies protect against acetaminophen-induced liver injury in mice. *Journal of Xenobiotics*, *1*(1), e8. https://doi.org/10.4081/xeno.2011.e8

Chang, Y. C., Yuan, L., Liu, J. R., Muhammad, I., Cao, C. B., Shi, C. X., Zhang, Y. Y., Li, R., Li, C. W., & Liu, F. P. (2020). Dihydromyricetin attenuates *Escherichia coli* lipopolysaccharide-induced ileum injury in chickens by inhibiting NLRP3 inflammasome and TLR4/NF-κB signalling pathway. *Veterinary Research*, *51*(72), 1–12. https://doi.org/10.1186/s13567-020-00796-8

Couteur, D., Rivory, L. P., & Pond, S. M. (1996). The effect of oxidative injury on hepatocellular influx of leucine in the rat. *International Hepatology Communications*, *4*(6), 343–350. https://doi.org/10.1016/0928-4346(96)00266-6

Ding, R. J., Ning, S. Y., Yang, X. L., Shi, J. C., Zhao, S. J., Zhang, A. R., Gao, X. X., Tian, J. S., Zhang, B., & Qin, X. M. (2022). Brain and testicular metabonomics revealed the protective effects of Guilingji on senile sexual dysfunction rats. *Journal of Ethnopharmacology*, 115047. https://doi.org/10.1016/j.jep.2022.115047

Du, X. W., Wang, X. L., Jiang, D. Y., Geng, N. Z., Zhang, S. C., Zhou, Y. Y., & Liu, C. J. (2013). Metabolomic study on the hepatoprotective effects of modified Sinisan using ultra-performance liquid chromatography/electrospray ionization quadruple time-of-flight mass spectrometry coupled with pattern recognition approach. *Analytical Methods-UK.*, *5*(11), 2727–2735. https://doi.org/10.1039/c3ay40143j

Fan, X. Y., Wang, L. D., Huang, J. B., Lv, H. M., Deng, X. M., & Ci, X. X. (2018). Pterostilbene reduces acetaminophen-induced liver injury by activating the nrf2 antioxidative defense system via the ampk/akt/gsk3β pathway. *Cellular Physiology and Biochemistry*, *49*(5), 1943–1958. https://doi.org/10.1159/000493655

Gao, Y., Li, J. T., Li, X., Li, X., Yang, S. W., Chen, N. H., Li, L., & Zhang, L. (2021). Tetrahydroxy stilbene glycoside attenuates acetaminophen-induced hepatotoxicity by UHPLC–Q-TOF/MS-based metabolomics and multivariate data analysis. *Journal of Cellular Physiology*, *236*(5), 3832–3862. https://doi.org/10.1002/jcp.30127

Glavinas, H., Krajcsi, P., Cserepes, J., & Sarkadi, B. (2004). The role of ABC transporters in drug resistance, metabolism and toxicity. *Current Drug Delivery*, *1*(1), 27–42. https://doi.org/10.2174/1567201043480036

Guo, M., Yang, X. L., & Schimmel, P. (2010). New functions of aminoacyl-tRNA synthetases beyond translation. *Journal Nature Reviews Molecular Cell Biology*, *11*(9), 668–674. https://doi.org/10.1038/nrm2956

He, J. (2019). *Intervention effect of polysaccharides from different processed products of Angelica sinensis on chicken liver injury induced by ceftiofur sodium combined with LPS*. Gansu Agricultural University.

Hua, Y. L., Ma, Q., Zhang, X. S., Yao, W. L., Ji, P., Hu, J. J., & Wei, Y. M. (2019). Urinary metabolomics analysis reveals the effect of volatile oil from *Angelica sinensis* on LPS-induced inflammation rats. *Biomedical Chromatography*, *33*(2), e4402. https://doi.org/10.1002/bmc.4402

Li, L., Yao, D. N., Lu, Y., Deng, J. W., Wei, J. A., Yan, Y. H., Deng, H., Han, L., & Lu, C. J. (2020). Metabonomics study on serum characteristic metabolites of psoriasis vulgaris patients with blood-stasis syndrome. *Frontiers in Pharmacology*, *11*, 558731. https://doi.org/10.3389/fphar.2020.558731

Li, Q., Liu, Y. L., Che, Z. Q., Zhu, H. L., Meng, G. Q., Hou, Y. Q., Ding, B. Y., Yin, Y. L., & Chen, F. (2012). Dietary L-arginine supplementation alleviates liver injury caused by *Escherichia coli* LPS in weaned pigs. *Innate Immunity*, *18*(6), 804–814. https://doi.org/10.1177/1753425912441955

Lieber, C. S., Casini, A., DeCarli, L. M., Kim, C. I., & Lowe, M. A. (1990). *S*-Adenosyl-L-methionine attenuates alcohol-induced liver injury in the baboon. *Hepatology*, *11*(2), 165–172. https://doi.org/10.1002/hep.1840110203

Liu, S. L., Ji, P., Wei, Y. M., He, J., Li, C. C., Hua, Y. L., Yao, W. L., Zhang, X. S., & Yuan, Z. W. (2020). Establishment of liver injury model induced by ceftiofur sodium combined with lipopolysaccharide in layer chicken. *Preventive Veterinary Medicine*, *41*, 86–90. https://doi.org/10.16437/j.cnki.1007-5038.2020.10.015

Lu, X. Y., Tian, Y., Lian, X. P., Jin, Y. C., Jin, T. T., Zhao, Q. Q., Hu, B., Shen, X. P., & Fan, X. H. (2014). Integrated systems toxicology approaches identified the possible involvement of ABC transporters pathway in erythromycin estolate-induced liver injury in rat. *Food and Chemical Toxicology*, *65*, 343–355. https://doi.org/10.1016/j.fct.2013.12.050

Ma, P., Sun, C. Y., Li, W. J., Deng, W. W., Adu-Frimpong, M., Yu, J. N., & Xu, X. M. (2020). Extraction and structural analysis of *Angelica sinensis* polysaccharide with low molecular weight and its lipid-lowering effect on nonalcoholic fatty liver disease. *Food Science & Nutrition*, *8*(7), 3212–3224. https://doi.org/10.1002/fsn3.1581

Morgan, M. Y., Milsom, J. P., & Sherlock, S. (1978). Plasma ratio of valine, leucine and isoleucine to phenylalanine and tyrosine in liver disease. *Gut*, *19*(11), 1068–1073. https://doi.org/10.1136/gut.19.11.1068

Mounet, F., Martine, L. C., Mickaël, M., Cécile, C., Jean-Luc, G., Catherine, D., René, L., Philippe, G., Anne, B., Monique, G., Christophe, R., Dominique, R., & Annick, M. (2007). Quantitative metabolic profiles of tomato flesh and seeds during fruit development: Complementary analysis with ANN and PCA. *Metabolomics*, *3*(3), 273–288. https://doi.org/10.1007/s11306-007-0059-1

Nagai, H., Shimazawa, T., Yakuo, I., Aoki, M., Koda, A., & Kasahara, M. (1989). The role of thromboxane a2 [TXA2] in liver injury in mice. *Prostaglandins*, *38*(4), 439–446. https://doi.org/10.1016/0090-6980(89)90126-3

Naghizadeh, M., Torshizi, M. A. K., Rahimi, S., Engberg, R. M., & Dalgaard, T. S. (2019). Effect of serum anti-phage activity on colibacillosis control by repeated phage therapy in broilers. *Veterinary Microbiology*, *234*, 61–71. https://doi.org/10.1016/j.vetmic.2019.05.018

Park, B. S., Yeo, S. G., Jung, J., & Na, Y. J. (2015). A novel therapeutic target for peripheral nerve injury-related diseases: Aminoacyl-tRNA synthetases. *Neural Regeneration Research*, *10*(10), 1656–1662. https://doi.org/10.4103/1673-5374.167766

Peng, S. L., Zhao, Y., Gu, X., Huang, Y., & Dai, C. L. (2008). The effects of Shenfu injection on liver injury after ischemia-reperfusion in rats. *Journal of Shanxi Medical*, *37*(10), 1284–1287. https://doi.org/10.3969/j.issn.1000-7377.2008.10.004

Prabhakar, S., & Ibrahim, R. S. (2015). Modulation effects of curcumin on erythrocyte ion-transporter activity. *International Journal of Cell Biology*, *2015*, 1–8. https://doi.org/10.1155/2015/630246

Sánchez-Illana, Á., Piñeiro-Ramos, J. D., Sanjuan-Herráez, J. D., Vento, M., Quintás, G., & Kuligowski, J. (2018). Evaluation of batch effect elimination using quality control replicates in LC–MS metabolite profiling. *Analytica Chimica Acta: X*, *1019*, 38–48. https://doi.org/10.1016/j.aca.2018.02.053

Subramanian, K., Selvakkumar, C., Meenakshisundaram, S., Balakrishnan, A., & Lakshmi, B. S. (2008). Extract of Alpinia officinarum suppresses enteropathogenic *Escherichia coli* (EPEC) lipopolysaccharide (LPS) induced inflammation in J774 a.1 macrophages. *Journal of Health Science*, *54*(1), 112–117. https://doi.org/10.1248/jhs.54.112

Tao, Y., Chen, X., Li, W. D., & Cai, B. C. (2017). Comparative analysis of 9 constituents in processed products of Radix Angelicae Sinensis. *Journal Traditional Chinese Drug Research and Clinical Pharmacology*, *28*(1), 88–92. https://doi.org/10.19378/j.issn.1003-9783.2017.01.019

Wan, M. Q., Liu, X. Y., Gao, H., Wang, T. X., Yang, Y. F., Jia, L. Y., Yang, X. W., & Zhang, Y. B. (2020). Systematic analysis of the metabolites of angelicae pubescentis radix by UPLC–Q-TOF–MS combined with metabonomics approaches after oral administration to rats. *Journal of Pharmaceutical and Biomedical*, *188*, 113445. https://doi.org/10.1016/j.jpba.2020.113445

Wang, K., Wang, J., Song, M., Wang, H. X., Xia, N., & Zhang, Y. (2020). *Angelica sinensis* polysaccharide attenuates CCl_4-induced liver fibrosis via the IL-22/STAT3 pathway. *International Journal of Biological Macromolecules*, *162*, 273–283. https://doi.org/10.1016/j.ijbiomac.2020.06.166

Wang, L., Xiao-Min, X. U., Zhi-Wei, L. U., Liu, Y. Q., Zhang, L. Y., Ding, N., Jin-Peng, H. E., Zhang, Y. H., & Cheng-Hao, L. I. (2017). Research on protection of *Angelica sinensis* polysaccharides on liver injury of rats induced by x-ray radiation. *Chinese Traditional and Herbal Drugs*, *48*(20), 4284–4288. CNKI:SUN:ZCYO.0.2017-20-024

Wang, M., Xu, J., Zhang, Y., Yang, N., Ge, W. H., & Song, R. (2021). Integrated multiplatform-based metabonomics and network analysis to explore the mechanism of *Polygonum cuspidatum* on hyperlipidemia. *Journal of Chromatography B*, *1176*(1), 122769. https://doi.org/10.1016/j.jchromb.2021.122769

Wang, R. X., Sheps, J. A., & Ling, V. (2011). ABC transporters, bile acids, and inflammatory stress in liver cancer. *Current Pharmaceutical Biotechnology*, *12*(4), 636–646. https://doi.org/10.2174/138920111795163986

Wang, X. J., Zhang, A. H., Han, Y., Wang, P., Sun, H., Song, G. C., Dong, T. W., Yuan, Y., Yuan, X. X., Zhang, M., Xie, N., Zhang, H., Dong, H., & Dong, W. (2012). Urine metabolomics analysis for biomarker discovery and detection of jaundice syndrome in patients with liver disease. *Molecular & Cellular Proteomics*, *11*(8), 370–380. https://doi.org/10.1074/mcp.M111.016006

Wei, D., Wu, S. F., Liu, J., Zhang, X. Q., Guan, X. L., Gao, L., & Xu, Z. (2020). Theobromine ameliorates nonalcoholic fatty liver disease by regulating hepatic lipid metabolism via mTOR signaling pathway *in vivo* and *in vitro*. *Canadian Journal of Physiology and Pharmacology*, *7*, 1–39. https://doi.org/10.1139/CJPP-2020-0259

Westerhuis, J. A., Velzen, E. J. J. V., Hoefsloot, H. C. J., & Smilde, A. K. (2010). Multivariate paired data analysis: Multilevel PLSDA versus OPLSDA. *Metabolomics*, *6*(1), 119–128. https://doi.org/10.1007/s11306-009-0185-z

Xie, Z. Y., Chen, E., Ouyang, X. X., Xu, X. W., Ma, S. S., Ji, F. Y., Wu, D. X., Zhang, S. N., Zhao, Y. L., & Li, L. J. (2019). Metabolomics and cytokine analysis for identification of severe drug-induced liver injury. *J. Proteome. Res.*, 18(6). 2514-2524. *18*, 2514–2524. https://doi.org/10.1021/acs.jproteome.9b00047

Xu, D. L., Teng, X. Q., Guo, R., Shen, X. D., Wan, M. S., Li, G. X., Zhang, R. L., & Ge, M. (2020). Metabonomic analysis of hypophosphatemic laying fatigue syndrome in laying hens. *Theriogenology*, *156*(6), 222–235. https://doi.org/10.1016/j.theriogenology.2020.06.032

Yang, X. J., Deng, Y., Yang, Z. J., Li, S., Hai, Y. X., & Tian, Y. H. (2021). Understanding Radix Angelica Sinensis blood replenishing mechanisms

on blood deficiency rats based on a UPLC–Q/TOF–MS metabolomics and network pharmacology. *Records of Natural Products*, *15*(4), 267–280. https://doi.org/10.25135/rnp.224.21.01.1950

Yang, Y., Zhao, J., Song, X. Q., Li, L. F., Li, F. Q., Shang, J., & Wang, W. W. (2019). Amygdalin reduces lipopolysaccharide-induced chronic liver injury in rats by down-regulating pi3k/akt, jak2/stat3 and nf-κb signalling pathways. *Artificial Cells, Nanomedicine, and Biotechnology*, *47*(1), 2688–2697. https://doi.org/10.1080/21691401.2019.1634084

Yang, Y. X., Li, F. Y., Wei, S. Z., Liu, X. Y., Wang, Y. Y., Liu, H. H., Wang, J. B., Li, H., Cai, H., & Zhao, Y. (2019). Metabolomics profiling in a mouse model reveals protective effect of Sancao granule on con A-induced liver injury. *Journal of Ethnopharmacology*, *238*, 111838. https://doi.org/10.1016/j.jep.2019.111838

Ye, Y. N., Liu, E. S. L., Li, Y., So, H. L., Cho, C. C. M., Sheng, H. P., Lee, S. S., & Cho, C. H. (2001). Protective effect of polysaccharides-enriched fraction from *Angelica sinensis* on hepatic injury. *Life Sciences*, *69*(6), 637–646. https://doi.org/10.1016/S0024-3205(01)01153-5

Yin, P. Y., Mohemaiti, P., Chen, J., Zhao, X. J., Lu, X., Yimiti, A., Upur, H., & Xu, G. W. (2018). Serum metabolic profiling of abnormal savda by liquid chromatography/mass spectrometry. *Journal of Chromatography B*, *871*(2), 322–327. https://doi.org/10.1016/j.jchromb.2008.05.043

Yu, F., Li, H. L., Meng, Y., & Yang, D. (2013). Extraction optimization of *Angelica sinensis* polysaccharides and its antioxidant activity in vivo. *Carbohydrate Polymers*, *94*(1), 114–119. https://doi.org/10.1016/j.carbpol.2013.01.050

Yuan, Z. W., Zhong, L. J., Hua, Y. L., Ji, P., Yao, W. L., Ma, Q., Zhang, X. S., Wen, Y. Q., Yang, L. H., & Wei, Y. M. (2019). Metabolomics study on promoting blood circulation and ameliorating blood stasis: Investigating the mechanism of *Angelica sinensis* and its processed products. *Biomedical Chromatography*, *33*(4), e4457. https://doi.org/10.1002/bmc.4457

Zhang, J. Z., Gao, Y., Guo, H. Q., Ding, Y., & Ren, W. B. (2019). Comparative metabolome analysis of serum changes in sheep under overgrazing or light grazing conditions. *BMC Veterinary Research*, *15*(469), 1–10. https://doi.org/10.1186/s12917-019-2218-9

Zhang, W. D., Chen, Y., Jiang, H. H., Yang, J. X., Wang, Q., Du, Y. F., & Xu, H. J. (2020). Integrated strategy for accurately screening biomarkers based on metabolomics coupled with network pharmacology. *Talanta*, *211*, 120710. https://doi.org/10.1016/j.talanta.2020.120710

Zhang, Y., Shi, J., Fei, Q., Huang, Y., Zhu, F. X., Wang, J., Tang, D. Q., & Chen, B. (2020). Plasma and urine metabonomics coupled with UPLC–Q-TOF/MS and multivariate data analysis on potential biomarkers in anemia and hematinic effects of steamed notoginseng. *Journal Phytochemistry Letters*, *38*, 55–64. https://doi.org/10.1016/j.jpba.2020.113445

Zhou, B. G., Zhao, H. M., Lu, X. Y., Wang, X., Zou, Y., Xu, R., Yue, H. Y., Liu, Y., Zuo, Z. Y., & Liu, D. Y. (2017). Erzhi pill® repairs experimental liver injury via TSC/mTOR signaling pathway inhibiting excessive apoptosis. *Evidence-Based Complementary and Alternative*, *2017*, 5653643. https://doi.org/10.1155/2017/5653643

Zhou, Y., Xu, M., Liu, P., Liang, B. Y., Qian, M. N., Wang, H. C., Song, X. H., Nyshadham, P., Che, L., Calvisi, D. F., Li, F., Lin, S., & Chen, X. (2020). Mtorc2 signaling is required for liver regeneration in a cholestatic liver injury murine model. *The American Journal of Pathology*, *190*(7), 1414–1426. https://doi.org/10.1016/j.ajpath.2020.03.010

Zhu, J. J., Lu, T. F., Yue, S., Shen, X. D., Gao, F., Busuttil, R. W., Weglinski, J. W. K., Xia, Q., & Zhai, Y. (2015). Rapamycin protects livers from ischemia and reperfusion injury via both autophagy induction and mTORC2-AKT activation. *Transplantation*, *99*(1), 48–55. https://doi.org/10.1097/TP.0000000000000476

SUPPORTING INFORMATION

Additional supporting information may be found in the online version of the article at the publisher's website.

How to cite this article: Wu, F., Hu, Y., Ji, P., Li, C., & He, J. (2022). Metabonomics study on the hepatoprotective effect mechanism of polysaccharides from different processed products of *Angelica sinensis* on layer chickens based on UPLC–Q/TOF–MS/MS, multivariate statistical analysis and conjoint analysis. *Biomedical Chromatography*, *36*(6), e5362. https://doi.org/10.1002/bmc.5362